



RESEARCH ARTICLE

10.1029/2020JD034356

Special Section:

The Exceptional Arctic Polar Vortex in 2019/2020: Causes and Consequences

Chemical Evolution of the Exceptional Arctic Stratospheric Winter 2019/2020 Compared to Previous Arctic and Antarctic Winters

I. Wohltmann¹ , P. von der Gathen¹ , R. Lehmann¹, H. Deckelmann¹ , G. L. Manney^{2,3} , J. Davies⁴, D. Tarasick⁴, N. Jepsen⁵, R. Kivi⁶ , N. Lyall⁷, and M. Rex¹

¹Alfred Wegener Institute for Polar and Marine Research, Potsdam, Germany, ²NorthWest Research Associates, Socorro, NM, USA, ³New Mexico Institute of Mining and Technology, Socorro, NM, USA, ⁴Air Quality Research Division, Environment and Climate Change Canada, Downsview, ON, Canada, ⁵Danish Meteorological Institute, Copenhagen, Denmark, ⁶Space and Earth Observation Center, Finnish Meteorological Institute, Sodankylä, Finland, ⁷UK Met Office, Lerwick Observatory, Lerwick, UK

Key Points:

- The Arctic stratospheric winter 2019/2020 showed the lowest ozone mixing ratios ever observed and was one of the coldest on record
- Chemical evolution of the Arctic winter 2019/2020 was a hybrid between typical Arctic and typical Antarctic conditions
- Only an additional 21–46 h below PSC temperatures and in sunlight would have been necessary to reduce ozone to near zero locally

Correspondence to:

I. Wohltmann,
ingo.wohltmann@awi.de

Citation:

Wohltmann, I., von der Gathen, P., Lehmann, R., Deckelmann, H., Manney, G. L., Davies, J., et al. (2021). Chemical evolution of the exceptional Arctic stratospheric winter 2019/2020 compared to previous Arctic and Antarctic winters. *Journal of Geophysical Research: Atmospheres*, 126, e2020JD034356. <https://doi.org/10.1029/2020JD034356>

Received 2 DEC 2020
Accepted 18 AUG 2021

Author Contributions:

Conceptualization: I. Wohltmann
Formal analysis: I. Wohltmann
Methodology: I. Wohltmann
Software: I. Wohltmann
Validation: I. Wohltmann
Visualization: I. Wohltmann
Writing – original draft: I. Wohltmann

© 2021. The Authors.

This is an open access article under the terms of the [Creative Commons Attribution-NonCommercial-NoDerivs License](https://creativecommons.org/licenses/by/4.0/), which permits use and distribution in any medium, provided the original work is properly cited, the use is non-commercial and no modifications or adaptations are made.

Abstract The winter 2019/2020 showed the lowest ozone mixing ratios ever observed in the Arctic winter stratosphere. It was the coldest Arctic stratospheric winter on record and was characterized by an unusually strong and long-lasting polar vortex. We study the chemical evolution and ozone depletion in the winter 2019/2020 using the global Chemistry and Transport Model ATLAS. We examine whether the chemical processes in 2019/2020 are more characteristic of typical conditions in Antarctic winters or in average Arctic winters. Model runs for the winter 2019/2020 are compared to simulations of the Arctic winters 2004/2005, 2009/2010, and 2010/2011 and of the Antarctic winters 2006 and 2011, to assess differences in chemical evolution in winters with different meteorological conditions. In some respects, the winter 2019/2020 (and also the winter 2010/2011) was a hybrid between Arctic and Antarctic conditions, for example, with respect to the fraction of chlorine deactivation into HCl versus ClONO₂, the amount of denitrification, and the importance of the heterogeneous HOCl + HCl reaction for chlorine activation. The pronounced ozone minimum of less than 0.2 ppm at about 450 K potential temperature that was observed in about 20% of the polar vortex area in 2019/2020 was caused by exceptionally long periods in the history of these air masses with low temperatures in sunlight. Based on a simple extrapolation of observed loss rates, only an additional 21–46 h spent below the upper temperature limit for polar stratospheric cloud formation and in sunlight would have been necessary to reduce ozone to near zero values (0.05 ppm) in these parts of the vortex.

1. Introduction

After the discovery of the Antarctic ozone hole by Farman et al. (1985), the question arose why a similar phenomenon was not observed in the Arctic. In contrast to the Antarctic, ozone depletion in the Arctic is typically much less pronounced and shows a higher interannual variability. This is caused by the significantly higher stratospheric temperatures and higher dynamical activity in the Northern Hemisphere, which are associated with a more pronounced Brewer-Dobson circulation and more downwelling (e.g., Manney et al., 2011; Solomon, 1999; Solomon et al., 2014; Tegtmeier et al., 2008). In addition to less pronounced chemical depletion, ozone loss is more likely to be masked by transport of ozone in the Northern Hemisphere. On average, the variability of chemistry and transport contributes about equally to the interannual variability in Arctic polar ozone (Tegtmeier et al., 2008).

The Arctic stratospheric winter 2019/2020 was characterized by an unusually strong and long-lasting polar vortex and was the coldest winter ever observed in the Arctic stratosphere (e.g., Dameris et al., 2021; Lawrence et al., 2020; von der Gathen et al., 2021; Wohltmann et al., 2020). The winter showed the lowest ozone mixing ratios ever measured in the Arctic polar vortex (e.g., Manney et al., 2020; Wohltmann et al., 2020). In the most depleted parts of the vortex, mixing ratios as low as 0.13 ppm were observed locally (Wohltmann et al., 2020), which is comparable to typical minimum mixing ratios of 0.01–0.1 ppm detected in the Antarctic ozone hole (e.g., Solomon et al., 2014). Vortex-averaged ozone loss was one of the largest ever observed in the Arctic and only rivaled by the ozone loss in the cold winter 2010/2011 (Grooß & Müller, 2021; Manney et al., 2011, 2020; Wohltmann et al., 2020).

Conditions in individual cold winters can counteract the effect of the slow decline of ozone-depleting substances, which has reduced the stratospheric chlorine loading in 2020 by about 10% compared to the peak values observed around the year 2000 (e.g., WMO, 2018). A tendency of the coldest Arctic winters to become colder in recent decades has been suggested by several studies (Rex et al., 2004, 2006; Sinnhuber et al., 2011; Tilmes et al., 2006; von der Gathen et al., 2021), although this is controversial (e.g., Ivy et al., 2014; Lawrence et al., 2018; Rieder & Polvani, 2013). Large interannual variability in temperatures and the occurrence of similarly cold winters are expected to extend into the future (e.g., Bednarz et al., 2016; Langematz et al., 2014; von der Gathen et al., 2021). While estimates suggest that stratospheric ozone levels will return to pre-1980 conditions around 2035 in the Arctic and 2060 in the Antarctic (Dhomse et al., 2018; WMO, 2018), it is expected that individual cold winters can still lead to substantial ozone depletion in the future (Bednarz et al., 2016; von der Gathen et al., 2021). There is, however, considerable uncertainty in the future trend of Arctic stratospheric temperatures (e.g., Butchart et al., 2010; Langematz et al., 2014; von der Gathen et al., 2021). In the light of these results, it is of interest to examine how similar the conditions in 2019/2020 were to typical conditions in Antarctic winters or in average Arctic winters.

We examine the chemical evolution of the winter 2019/2020 using simulations of the global ATLAS Chemistry and Transport Model (CTM; Wohltmann & Rex, 2009; Wohltmann et al., 2010, 2017). Results are compared to simulations of the Arctic winters 2004/2005, 2009/2010, and 2010/2011 and of the Antarctic winters 2006 and 2011 to assess the differences in chemical evolution in winters with different meteorological conditions. Chlorine and bromine released from decomposition of man-made chlorofluorocarbons and other ozone-depleting substances in the upper atmosphere are responsible for anthropogenic ozone depletion (e.g., Solomon, 1999; WMO, 2018). Chlorine is transformed from inactive reservoir gases (HCl and ClONO₂) to active chlorine species on the surfaces of polar stratospheric clouds, which only form at very low temperatures in polar winter. With the return of sunlight, ozone is depleted by photochemical catalytic cycles. We will have a closer look at these processes and assess the differences in the winters examined.

In addition, we look at the causes of the pronounced ozone minimum of less than 0.2 ppm at about 450 K potential temperature that was observed in about 20% of the polar vortex area in 2019/2020 at the end of March and beginning of April (Wohltmann et al., 2020).

Section 2 contains the model description and presents the setup of the model runs. Sections 3 and 4 give a short overview of the measurement data and the meteorological situation. In Section 5, we discuss the chemical evolution of the winter 2019/2020 in comparison to other Arctic and Antarctic winters. In Section 6, we have a look at the causes of the pronounced ozone minimum observed in 2019/2020. Section 7 presents the conclusions.

2. Model

Simulations are performed with the global Lagrangian CTM ATLAS (Wohltmann & Rex, 2009; Wohltmann et al., 2010, 2017). The model includes a gas-phase stratospheric chemistry module, heterogeneous chemistry on polar stratospheric clouds, a particle-based Lagrangian denitrification module, and a dehydration parameterization. The chemistry module comprises 47 active species and more than 180 reactions. Absorption cross sections and rate coefficients are taken from recent Jet Propulsion Laboratory recommendations (Burkholder et al., 2019). In addition to the binary background aerosol, the model simulates three types of polar stratospheric clouds, that is, supercooled ternary HNO₃/H₂SO₄/H₂O solutions, and clouds composed of solid nitric acid trihydrate (NAT) particles or ice.

Model runs are driven by meteorological data from the European Center of Medium-Range Weather Forecasts (ECMWF) ERA5 reanalysis (provided on a 1.125° × 1.125° horizontal grid, 3 h temporal resolution, and 137 model levels; Hersbach et al., 2020). The model uses a hybrid vertical coordinate that is identical to a pure potential temperature coordinate for a pressure lower than 100 hPa. Diabatic heating rates from ERA5 are used to calculate vertical motion. The vertical range of the model domain is 350–1,900 K and the horizontal resolution of the model is 150 km (mean distance between air parcels). Vertical resolution is about 40 K potential temperature in the lower stratosphere.

The model run for 2019/2020 starts on September 1, 2019 and ends on May 1, 2020. Model data before October 1, 2019 are not used to allow for a spin up of the mixing in the model. Additional runs with the same setup are performed for the Arctic winters 2004/2005, 2009/2010, and 2010/2011 and for the Antarctic winters 2006 and 2011. All Arctic runs start on September 1 of the respective starting year, and all Antarctic runs start on April 1 and do not use data before May 1.

The chemical species are initialized on October 1 of the respective starting year for the Arctic runs and on May 1 for the Antarctic runs. O_3 , H_2O , HCl , N_2O , HNO_3 , and CO are initialized from all individual measurements of the Microwave Limb Sounder (MLS) satellite instrument (version 4.2 data, Livesey et al., 2020) on the day of the model initialization by interpolation. $ClONO_2$ is initialized from a climatology (2004–2013) of the ACE-FTS satellite instrument as a function of pressure and equivalent latitude for the month of October (Arctic runs) or May (Antarctic runs; Koo et al., 2017). We did not correct $ClONO_2$ for the trend in Cl_y between 2004 and 2013 and the respective years of the model runs. The corresponding correction would have been smaller than 0.1 ppb in all cases and was deemed to be negligible. The change in total chlorine in the time period 2004–2020 is about 5% (WMO, 2018) and is mostly taken into account by the initialization with actual measurements of HCl by MLS. Even if this change was not taken into account, it would have only a small effect on the results.

$BrONO_2$ is assumed to contain all Br_y , which is taken from a Br_y-CH_4 relationship from ER-2 aircraft and Triple balloon data (Grooß et al., 2002). All Br_y values are scaled with a constant factor to give maximum values of 19.9 ppt for the year of measurement (2000; Dorf et al., 2008). Then, Br_y is scaled to take into account the trends in Br_y and CH_4 between the measurement date and the start dates of the model runs (WMO, 2018). CH_4 and NO_x are initialized as described in Wohltmann et al. (2017). The setup for the parameters of the polar stratospheric cloud model (e.g., number densities, supersaturation, and nucleation rate) is the same as described in Wohltmann et al. (2017).

A well-known deficiency of most CTMs is a marked discrepancy between measured and modeled HCl mixing ratios in the polar vortices (e.g., Brakebusch et al., 2013; Grooß et al., 2018; Solomon et al., 2015; Wohltmann et al., 2017), which is particularly pronounced in the Antarctic vortex. This points to a lack of understanding of the processes determining HCl in the polar vortices (Grooß et al., 2018; Wohltmann et al., 2017). To improve the agreement between model and measurements, a temperature offset of -3 K for the calculation of the Henry constant of HCl is used as an empirical correction. It is important to note here that while this correction improves the agreement between measurements and model (see Figures 21 and 22 of Wohltmann et al., 2017), discrepancies remain (see discussion in the following sections). The underlying causes for the discrepancy are still unknown (Grooß et al., 2018; Wohltmann et al., 2017), and the correction can only be empirical. The effect on ozone loss is small (Grooß et al., 2018; Wohltmann et al., 2017).

3. Measurement Data

In Section 6, we use the same set of 52 ozone sonde profiles measured inside the polar vortex from March 17 to April 17, 2020 as in Wohltmann et al. (2020). The precision of the ozone sondes is $\pm(3-5)\%$ and the accuracy is $\pm(5-10)\%$ (Smit et al., 2007). For small values of the ozone mixing ratio, the background current of the sonde and its subtraction handling become important. An assumed 20% uncertainty in the background subtraction in the minimum region converts to a range of 0.002–0.02 ppm, which is usually in the range of $\pm(5-10)\%$ and below.

In addition, we use satellite observations of ozone, HCl , HNO_3 , and ClO from MLS for validation (version 4.2 data, Livesey et al., 2020). The accuracy of the measurements is indicated in the respective figures. For the vortex averages, the random errors of the MLS measurements are negligible.

4. Overview of the Meteorological Evolution of the Winter 2019/2020

Detailed accounts of the evolution of the polar vortex, temperatures, and measured chemical species in the stratospheric Arctic winter 2019/2020 can be found in Lawrence et al. (2020) and Manney et al. (2020), and we will only give a short overview. A discussion of the temperatures and meteorological conditions of the

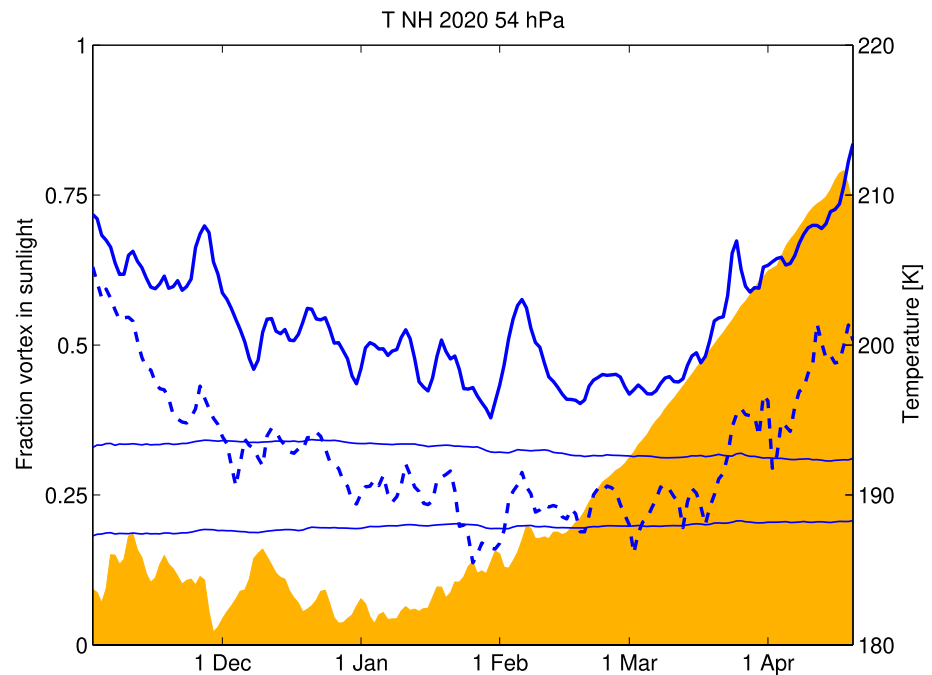


Figure 1. Vortex-averaged temperature (blue), vortex minimum temperature (dashed blue), and fraction of the vortex area in sunlight (yellow) at 54 hPa for the Arctic winter 2019/2020. The upper thin blue line shows the upper temperature limit for the formation of nitric acid trihydrate (NAT) clouds inferred from the ATLAS model and the lower thin blue line shows the same for ice clouds.

other winters examined in this manuscript can be found in, for example, Lawrence et al. (2020), Wohltmann et al. (2020) (e.g., Figure 1), or Wohltmann et al. (2017).

Figure 1 shows the evolution of the vortex-averaged temperatures and sunlit portion of the vortex for the winter 2019/2020. The vortex edge is assumed at 36 PVU potential vorticity at 475 K (e.g., Rex et al., 1999). The vortex edge criterion was extended to other altitudes by the modified potential vorticity of Lait (1994). The winter 2019/2020 was characterized by an unusually strong, long-lasting, and cold polar vortex (Lawrence et al., 2020). Temperatures dropped below the upper temperature limit for the formation of NAT clouds (T_{NAT}) around December 1 and remained below T_{NAT} in significant parts of the vortex until the end of March. At this date, the cold region reached from 370 to 550 K. At the end of March, temperatures rose quickly above T_{NAT} , leading to an abrupt end of conditions favorable for chlorine activation and ozone depletion. Temperatures below the threshold for ice cloud formation (T_{ice}) were occasionally observed. The lowest temperatures in 2020 were detected around February 1. This led to the formation of ice clouds visible as a decline in the MLS water vapor measurements (Manney et al., 2020).

5. Chemical Evolution of the 2019/2020 Winter and Comparison to Other Winters

In this section, we discuss the chemical evolution of the 2019/2020 winter and compare the results to other Arctic and Antarctic winters. In most cases, we limit our study to polar vortex means and the 54 hPa pressure level to keep the discussion at a reasonable length. The 54 hPa level is in a representative altitude for anthropogenic ozone depletion and is one of the levels studied in Wohltmann et al. (2017), which allows direct comparison to figures in Wohltmann et al. (2017) that show additional years and results for both the Northern and Southern Hemisphere. 54 hPa is not a material surface and this implies that we look at different air masses at different points of time. However, other choices such as a potential temperature surface or a surface following the mean descent in the vortex are not material surfaces either, and there is no straightforward way to follow the same air masses over the course of a complete winter (and, e.g., to

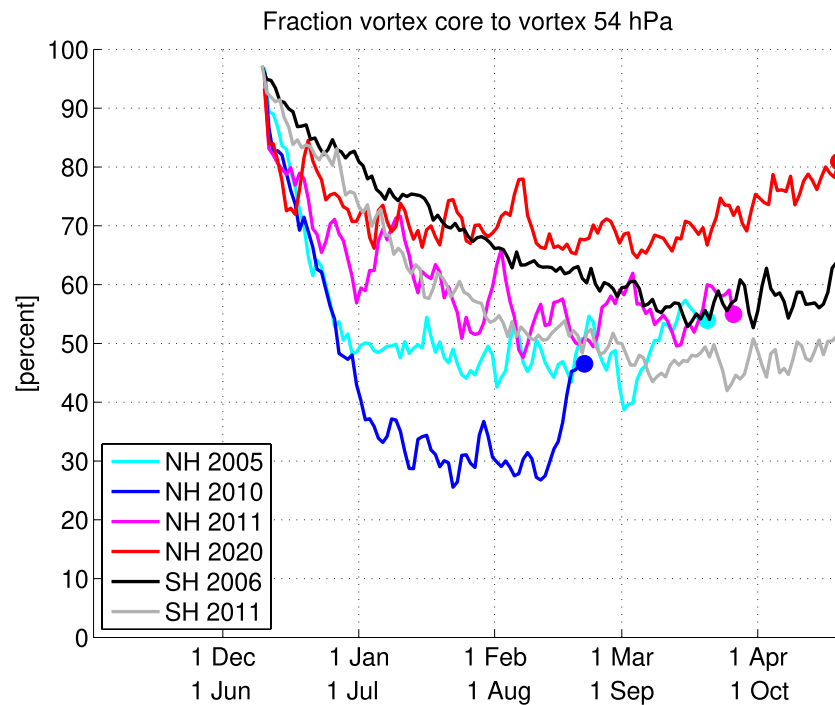


Figure 2. Fraction of the vortex area that meets the condition of being in the vortex core according to the definition in the text (values of the “vortex tracer” greater than 0.7) at 54 hPa for the Arctic winters 2004/2005, 2009/2010, 2010/2011, and 2019/2020 and for the Antarctic winters 2006 and 2011. Antarctic values are shifted by half a year. Dots show the approximate breakup date of the Arctic polar vortex (see Section 5).

stay inside the vortex and in a reasonable altitude range at the same time). A similar approach is taken, for example, in Solomon et al. (2014).

The results for the Arctic winter 2019/2020 are compared to the Arctic winters 2004/2005, 2009/2010, and 2010/2011. While the winters 2004/2005 and 2009/2010 are examples of winters with average temperatures and ozone depletion for the past 15 years, the winter 2010/2011 was the second coldest Arctic stratospheric winter after the 2019/2020 winter (Lawrence et al., 2020; Wohltmann et al., 2020) and showed a comparable amount of vortex-averaged ozone depletion (Manney et al., 2020; Wohltmann et al., 2020). Results are also compared to the Antarctic winters 2006 and 2011 to examine how different the conditions in the Arctic winters were from Antarctic conditions.

The vortex edge is assumed to be at a modified potential vorticity of 36 PVU at 475 K in the Northern Hemisphere and at -36 PVU at 475 K in the Southern Hemisphere. We only discuss vortex means before the breakup date of the vortex. The approximate breakup date of the vortex is calculated as the first date in spring when the area of the vortex at 54 hPa decreases below 15 million km². In the Antarctic winters, the breakup date is later than the last date shown in the plots. Since there are often notable differences between the vortex core and the vortex edge, which is more affected by sunlight and mixing, we show both averages over the complete vortex and the core of the vortex. To accomplish this, we initialize a “vortex tracer” as an artificial species on December 10 in the Northern Hemisphere and on June 10 in the Southern Hemisphere, which is set to 1 inside the vortex and to 0 outside the vortex. The vortex tracer is then transported and mixed in the model and can take any value between 0 and 1. We only include air parcels in the mean for the vortex core for which the vortex tracer has a value greater than 0.7 (see Wohltmann et al., 2017). Figure 2 shows the fraction of the vortex area that meets the condition of being in the vortex core at 54 hPa for the discussed Arctic and Antarctic winters.

5.1. Chlorine Activation and Deactivation

Figure 3 shows the modeled vortex-averaged mixing ratios of active chlorine ClO_x (a, b) at 54 hPa for the different Arctic and Antarctic winters. In addition, the figure shows the reservoir gases HCl (c, d) and ClONO_2 (e, f). Figures 3a, 3c and 3e show vortex means and Figures 3b, 3d and 3f show means over the vortex core. In 2019/2020, significant vortex-averaged chlorine activation (>0.1 ppb) was seen in the model from November 24 to March 29 at 54 hPa (Figure 3a). Chlorine activation in November is unusually early and is normally not observed before the start of December in other Arctic winters (Figure 3a, see also Manney et al., 2020). The early chlorine activation was caused by record low temperatures in November and early December (Lawrence et al., 2020; Wohltmann et al., 2020). In the inner parts of the vortex, ClO_x reached peak values of 2.4 ppb at 54 hPa (Figure 3b). Chlorine activation is also indicated by the decreasing mixing ratios of HCl and ClONO_2 (Figures 3c–3f).

The temporal increase in ClO_x is more pronounced in the average Arctic winters than in the Antarctic winters in the vortex core (see Figure 3b), likely because of stronger downwelling by the Brewer-Dobson circulation. The winter 2019/2020 showed a stable and cold vortex with weak transport (e.g., Lawrence et al., 2020). Nevertheless, simulated ClO_x values are higher in 2019/2020 than in any other simulated Arctic winter, presumably because of the colder conditions. In general, simulated ClO_x values in the Northern Hemisphere are higher than or comparable to the values in the Southern Hemisphere during the period when there is a stable vortex in the Northern Hemisphere (Figures 3a and 3b). This may be caused not only by differences in downwelling but also by more severe overestimation of HCl in the model in the Southern Hemisphere. This is discussed in more detail at the end of this section and in Section 5.3. However, for the amount of ozone depletion, the time period when high ClO_x values are observed is of critical importance (e.g., Solomon et al., 2014), and in average Arctic winters, this time period is several weeks to months shorter than in the Southern Hemisphere (Figures 3a and 3b).

Figure 4 shows the chemical reaction rates of all reactions involving HCl and ClONO_2 averaged over the vortex core for the winter 2019/2020. In a first activation phase ending in December, HCl and ClONO_2 were transformed into ClO_x by the reaction $\text{HCl} + \text{ClONO}_2$ until most available ClONO_2 was consumed. In individual air masses, this step proceeds rather rapidly, usually within less than 1 day (e.g., ATLAS simulations on example trajectories in Figures 8–13 by Nakajima et al., 2016). The second phase, which started in mid-January and lasted until mid of March, was characterized by a competition between activation and deactivation (see also, e.g., Portmann et al., 1996; Solomon et al., 2015). There are both activation and deactivation reactions that depend on sunlight and their rates increase with increasing illumination. Note that under certain conditions, activation and deactivation reactions may not be independent of each other and may exactly cancel out (Müller et al., 2018). Activation by the reactions $\text{HCl} + \text{ClONO}_2$ and $\text{HOCl} + \text{HCl}$ was about equally important in this phase. In this respect, the winters 2019/2020 and 2010/2011 (not shown) were a hybrid between Arctic and Antarctic conditions: In the Southern Hemisphere, activation later in winter is normally dominated by $\text{HOCl} + \text{HCl}$ because of a lack of NO_x , while in average winters in the Northern Hemisphere, like 2004/2005, $\text{HOCl} + \text{HCl}$ usually plays a smaller role because of the less severe denitrification (e.g., Crutzen et al., 1992; Grooß et al., 2011; Prather, 1992; Wohltmann et al., 2017). The activation in this time period (until mid-March) was nearly balanced by deactivation. Deactivation in this time period via $\text{Cl} + \text{CH}_4$ into HCl and via $\text{ClO} + \text{NO}_2$ into ClONO_2 was about equally important in the vortex core (Figure 4). The mixing ratios of HCl and ClONO_2 did not change significantly because of the quick reactivation into active chlorine (green lines in Figures 3d, 3f and 4). Figures corresponding to Figure 4 that complement these results for additional years, for the northern and Southern Hemisphere, and for different altitude levels can be found in Wohltmann et al. (2017) (e.g., their Figures 13a, 13b, 17a, and 17b and supplement).

Figures 3a and 3b show that a significant decrease of ClO_x starts around mid-March in 2019/2020. A quick rise of temperatures at the end of March led to an abrupt end of chlorine activation and a quick deactivation of chlorine into the reservoir gases, see also Manney et al. (2020). Both deactivation into HCl and into ClONO_2 are seen (Figures 3c–3f). Typically, chlorine deactivation in the Arctic proceeds into ClONO_2 via the reaction $\text{ClO} + \text{NO}_2$, while chlorine deactivation into HCl by the reaction $\text{Cl} + \text{CH}_4$ is the predominant deactivation pathway under low ozone levels and denitrified conditions in the Antarctic ozone hole (e.g., Douglass et al., 1995; Oelhaf et al., 1994; Portmann et al., 1996; Wohltmann et al., 2017). Figures 3c–3f show that

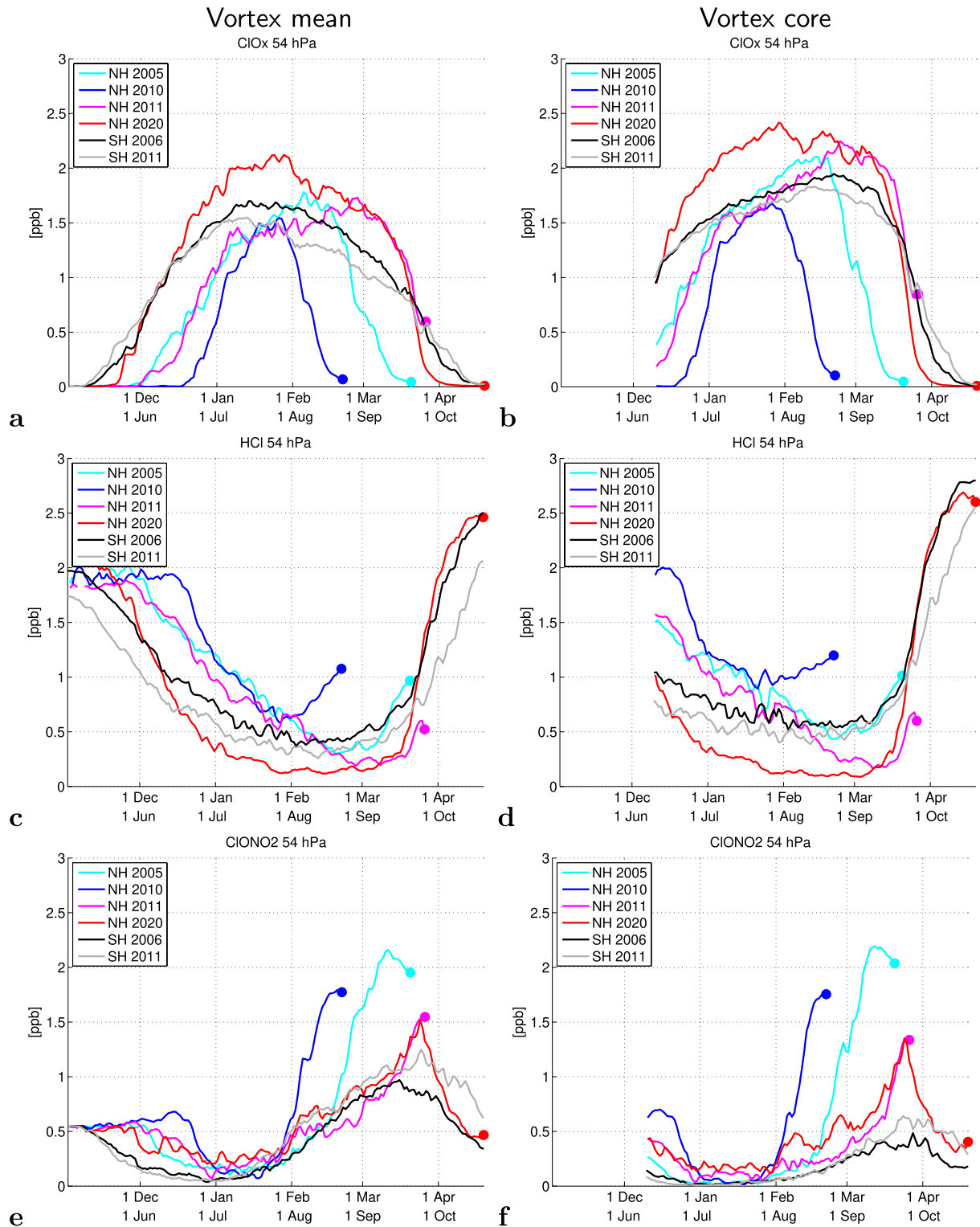


Figure 3. Modeled mixing ratios of active chlorine ClO_x (a and b), HCl (gas phase, c, d), and ClONO_2 (e and f) in the polar vortex at 54 hPa for the Arctic winters 2004/2005, 2009/2010, 2010/2011, and 2019/2020 and for the Antarctic winters 2006 and 2011. (a, c, e) Vortex means and (b, d, f) Means over the polar vortex core. Antarctic values are shifted by half a year. Dots show the approximate breakup date of the Arctic polar vortex (see Section 5).

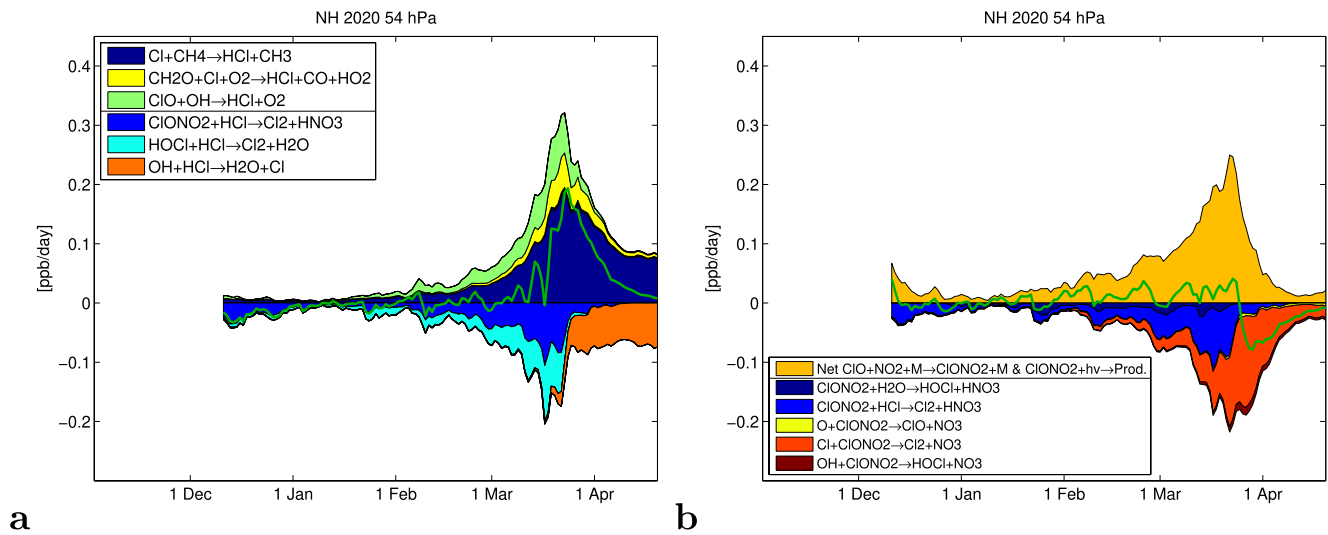


Figure 4. Chemical reaction rates of HCl and ClONO₂ in the polar vortex core at 54 hPa for the Arctic winter 2019/2020 with production/loss for each reaction added on to the previous one shown. (a) Vortex-averaged chemical reaction rates involving HCl. Production reactions show positive values and are separated by a line in the legend from the loss reactions, which show negative values. The net change of HCl is shown as a green line. (b) Same for ClONO₂. The net production rate of the fast cycle $\text{ClO} + \text{NO}_2 + \text{M} \rightarrow \text{ClONO}_2 + \text{M} / \text{ClONO}_2 + h\nu \rightarrow \text{products}$ is shown. This cycle is separated by a line in the legend from the loss reactions.

for the average Arctic winters 2004/2005 and 2009/2010 deactivation mainly proceeds into ClONO₂ while for the Antarctic winters in the vortex core, deactivation mainly proceeds into HCl (Figures 3d and 3f). There is also some deactivation into ClONO₂ in Antarctic winters at the vortex edge, which might be due to transport of NO_x into the vortex (Figure 3e). Some of the increase in HCl in the Northern Hemisphere in spring is due to transformation of ClONO₂ into HCl (Figure 4).

Again, the winters 2010/2011 and 2019/2020 show conditions somewhere in between average Arctic winters and Antarctic winters: In these years, deactivation into both ClONO₂ and HCl is observed in the model. This is particularly apparent in the ClONO₂ mixing ratios in the vortex core (Figure 3f). It is likely that deactivation proceeds into HCl at some locations and into ClONO₂ at other locations in these winters. Deactivation into HCl requires low ozone values and denitrified conditions, while deactivation into ClONO₂ requires NO_x. To some extent, these conditions for the deactivation pathways exclude each other. Even though we are looking at vortex averages, this is visible in Figures 3c–3f. The vortex core shows more deactivation into HCl and less into ClONO₂ than the complete vortex. This is due to higher values of ozone and NO_x at the vortex edge. Examples for deactivation into HCl and ClONO₂ for individual trajectories are shown in Section 6 (Figure 17).

Figure 3d shows minimum HCl mixing ratios in the vortex core of about 0.5 ppb in the Antarctic. These are significantly higher than the mixing ratios of below 0.2 ppb simulated for the Arctic winters 2010/2011 and 2019/2020. The high HCl mixing ratios in the Antarctic are unrealistic and are related to the well-known discrepancy between HCl measurements and simulations in most CTMs (e.g., Brakebusch et al., 2013; Groß et al., 2018; Solomon et al., 2015; Wohltmann et al., 2017). Even though an empirical correction for this has been applied in the model runs (see model description), a discrepancy remains in the model (which would be even larger without the correction, see Wohltmann et al., 2017, Figures 21 and 22). Figure 5 shows a comparison of simulated vortex-averaged HCl mixing ratios with MLS observations. Simulated vortex averages show an overestimate of up to 0.4 ppb in the Northern Hemisphere compared with MLS measurements and of up to 0.6 ppb in the Southern Hemisphere. Local differences between model and measurements in the Antarctic vortex core can reach 1 ppb (not shown). However, the effect on ozone loss is small (Groß et al., 2018; Wohltmann et al., 2017) and the effect on active chlorine is less than expected (see Section 5.3 for more detailed discussion).

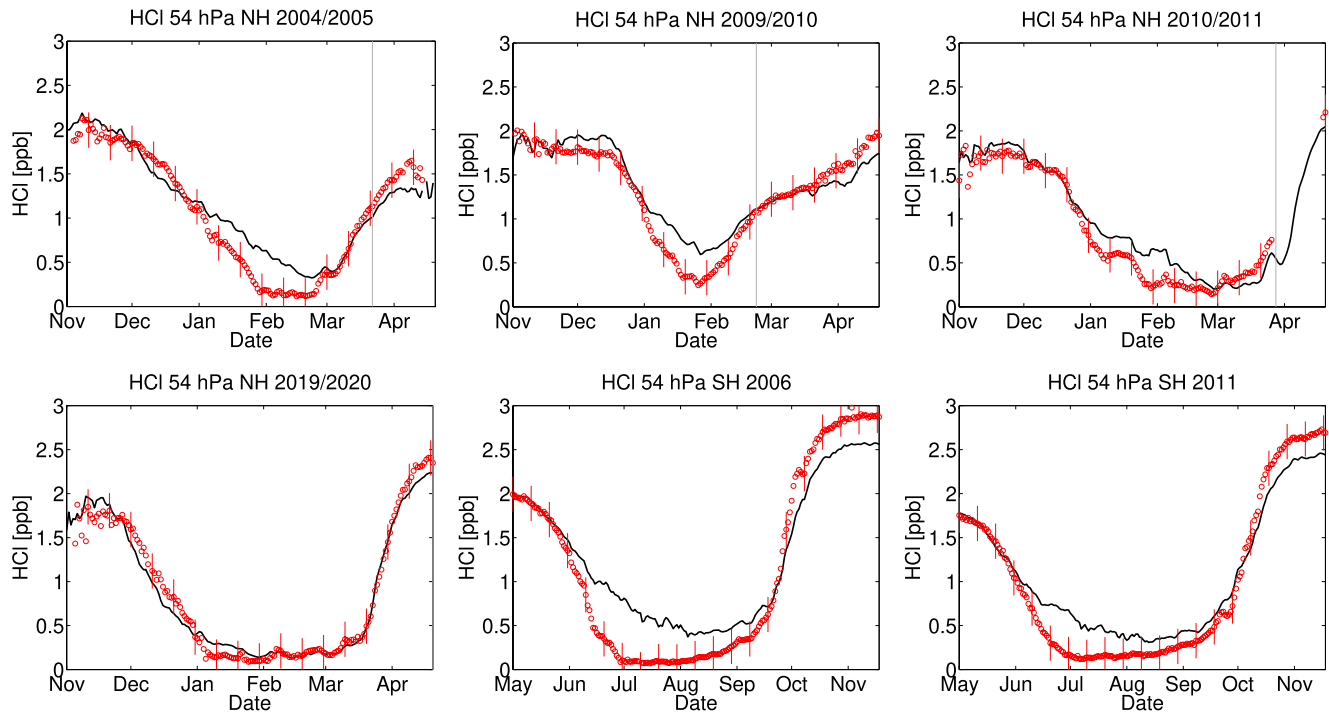


Figure 5. Modeled and observed HCl mixing ratios in the polar vortex at 54 hPa for the Arctic winters 2004/2005, 2009/2010, 2010/2011, and 2019/2020 and for the Antarctic winters 2006 and 2011. Modeled vortex averages (black) compared to corresponding vortex averages of the Microwave Limb Sounder (MLS) instrument (red, bars show the accuracy of the measurements). The gray line shows the approximate breakup date of the Arctic polar vortex (see Section 5).

5.2. HNO₃ and Denitrification

Denitrification and the amount of HNO₃ in the polar vortex can have a significant impact on the amount of ozone loss, for example, by impeding deactivation of active chlorine into ClONO₂. Figure 6 shows the modeled vortex-averaged mixing ratios of gas-phase HNO₃ at 54 hPa for the different Arctic and Antarctic

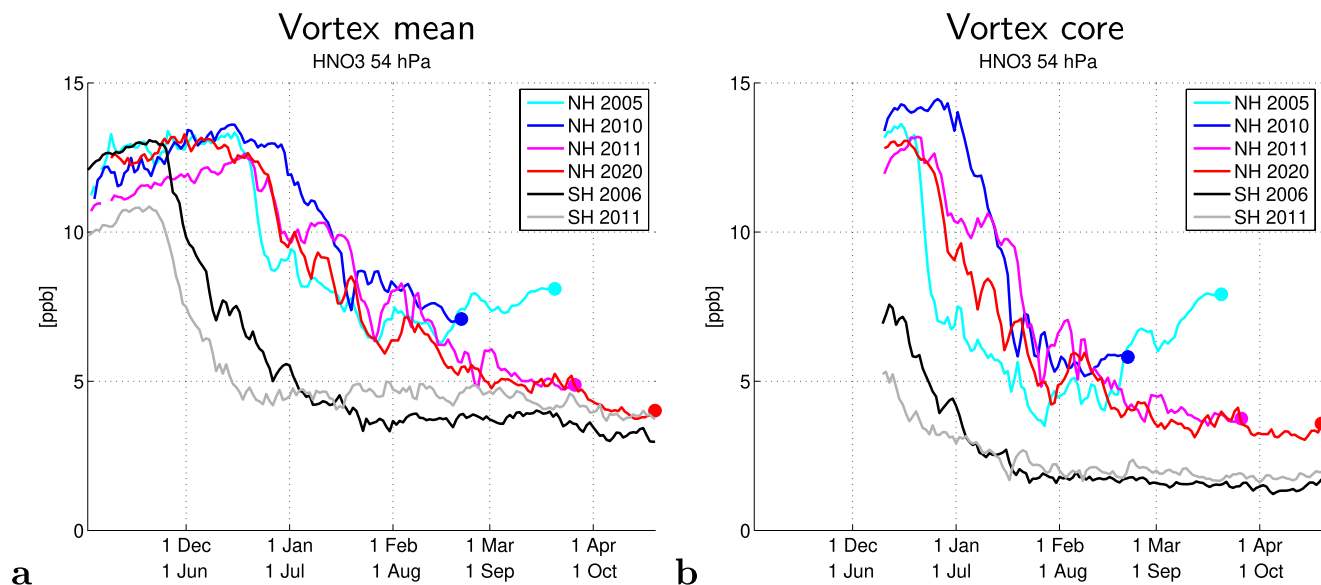


Figure 6. Modeled mixing ratios of gas-phase HNO₃ in the polar vortex at 54 hPa for the Arctic winters 2004/2005, 2009/2010, 2010/2011, and 2019/2020 and for the Antarctic winters 2006 and 2011. (a) Vortex means and (b) Means over the polar vortex core. Antarctic values are shifted by half a year. Dots show the approximate breakup date of the Arctic polar vortex (see Section 5).

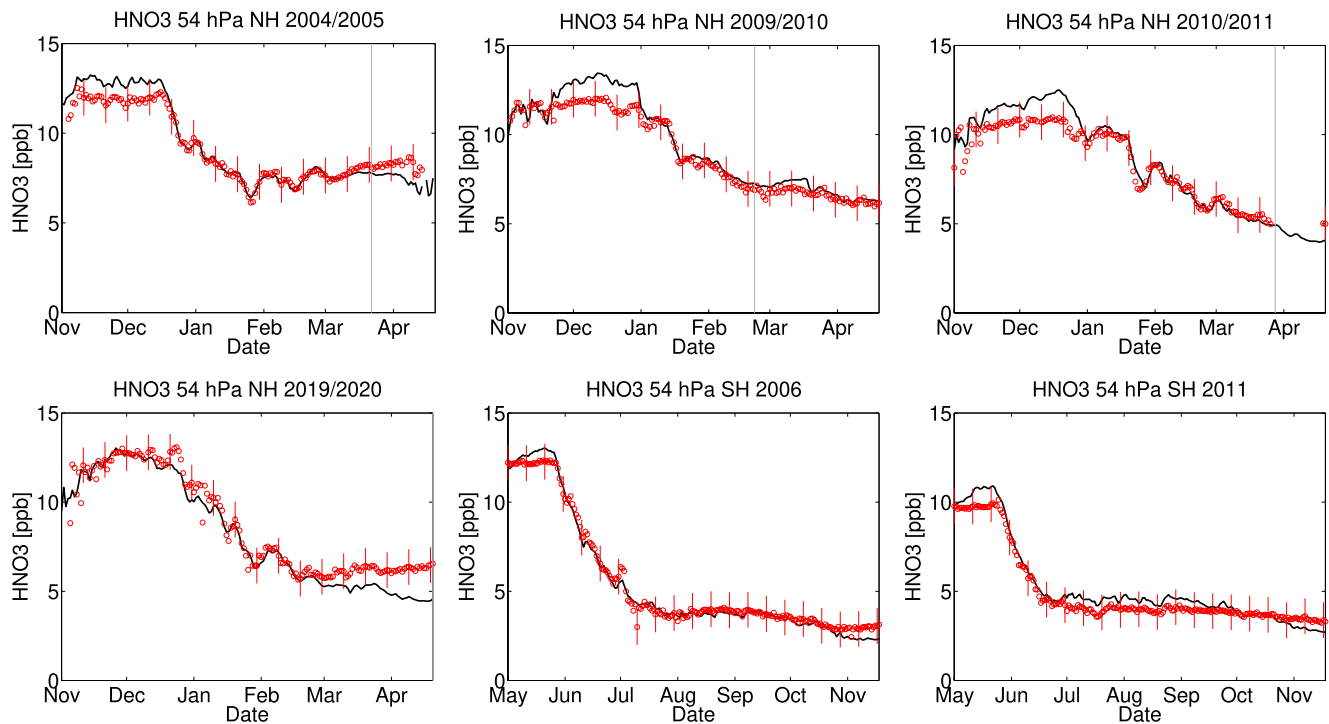


Figure 7. Modeled and observed gas-phase HNO_3 mixing ratios in the polar vortex at 54 hPa for the Arctic winters 2004/2005, 2009/2010, 2010/2011, and 2019/2020 and for the Antarctic winters 2006 and 2011. Modeled vortex averages (black) compared to corresponding vortex averages of the Microwave Limb Sounder instrument (red, bars show the accuracy of the measurements). The gray line shows the approximate breakup date of the Arctic polar vortex (see Section 5).

winters. Figure 6a shows vortex means and Figure 6b shows means over the vortex core. The general decrease of HNO_3 in all of the winters is mainly driven by denitrification by sedimenting PSC particles in the model (e.g., Wohltmann et al., 2017). At the end of the winter, vortex-averaged HNO_3 mixing ratios are comparable for the cold Arctic winters 2010/2011 and 2019/2020 and the Antarctic winters (about 3–5 ppb). However, these low values are approached much more quickly in the Southern Hemisphere (after about 1 month) than in the cold Arctic winters (after 4–5 months). The average Arctic winters show mixing ratios that are considerably higher (7–8 ppb).

In general, HNO_3 mixing ratios are lower in the vortex core than in the complete vortex. This is caused by the more pronounced denitrification due to the lower temperatures and by less in-mixing of air. In the Antarctic winters, the vortex core is almost completely denitrified with HNO_3 mixing ratios of about 2 ppb for more than 4 months, while the average Arctic winters show minimum HNO_3 values of 5–8 ppb. Once again, the winters 2010/2011 and 2019/2020 show conditions somewhere in between, with minimum HNO_3 values around 3.5 ppb at the end of the winter.

Figure 7 shows a comparison of simulated vortex-averaged gas-phase HNO_3 mixing ratios to MLS observations. In all years, the modeled vortex averages agree well with the MLS observations, which shows that denitrification is captured well by the model. The most notable difference is an underestimation of HNO_3 by the model in March and April 2020 by about 2 ppb.

5.3. Ozone

Figures 8a and 8b show the evolution of the vortex-averaged ozone mixing ratios at 54 hPa in the different Arctic and Antarctic winters. Initial mixing ratios on November 1 (or May 1, respectively) are about 2.5 ppm in all winters. By the end of the winter, vortex-averaged mixing ratios in the Antarctic winters and the cold Arctic winters decrease to values of 1–1.7 ppm, while the warmer Arctic winters show values of about 3.1–3.2 ppm. In the vortex core, mixing ratios fall even lower, with the Antarctic winters showing mixing ratios

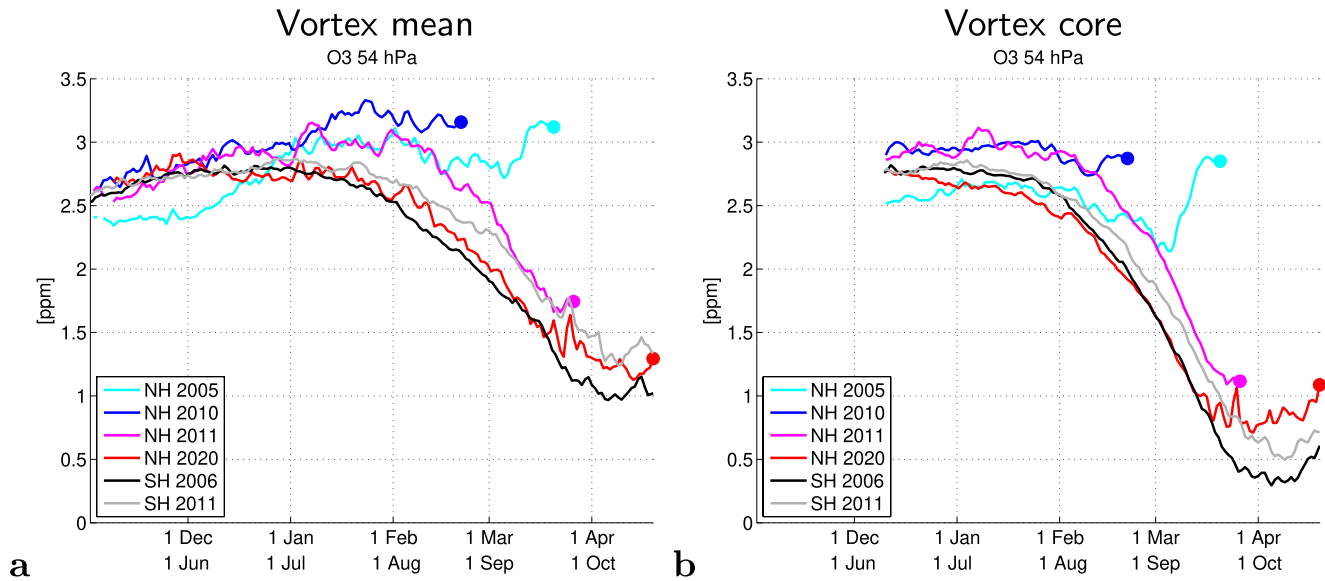


Figure 8. Ozone mixing ratios in the polar vortex at 54 hPa for the Arctic winters 2004/2005, 2009/2010, 2010/2011, and 2019/2020 and for the Antarctic winters 2006 and 2011. (a) Vortex means and (b) Means over the polar vortex core. Antarctic values are shifted by half a year. Dots show the approximate breakup date of the Arctic polar vortex (see Section 5).

of 0.6–0.7 ppm and the cold Arctic winters showing mixing ratios of about 1.1 ppm. Figure 9 shows a comparison of the simulated ozone mixing ratios to MLS observations. In all years, the modeled vortex averages agree with vortex averages observed by MLS within 0.4 ppm (corresponding to 20% maximum difference in the Northern Hemisphere and 30% in the Southern Hemisphere). Typically, ATLAS overestimates ozone somewhat at the end of the winter.

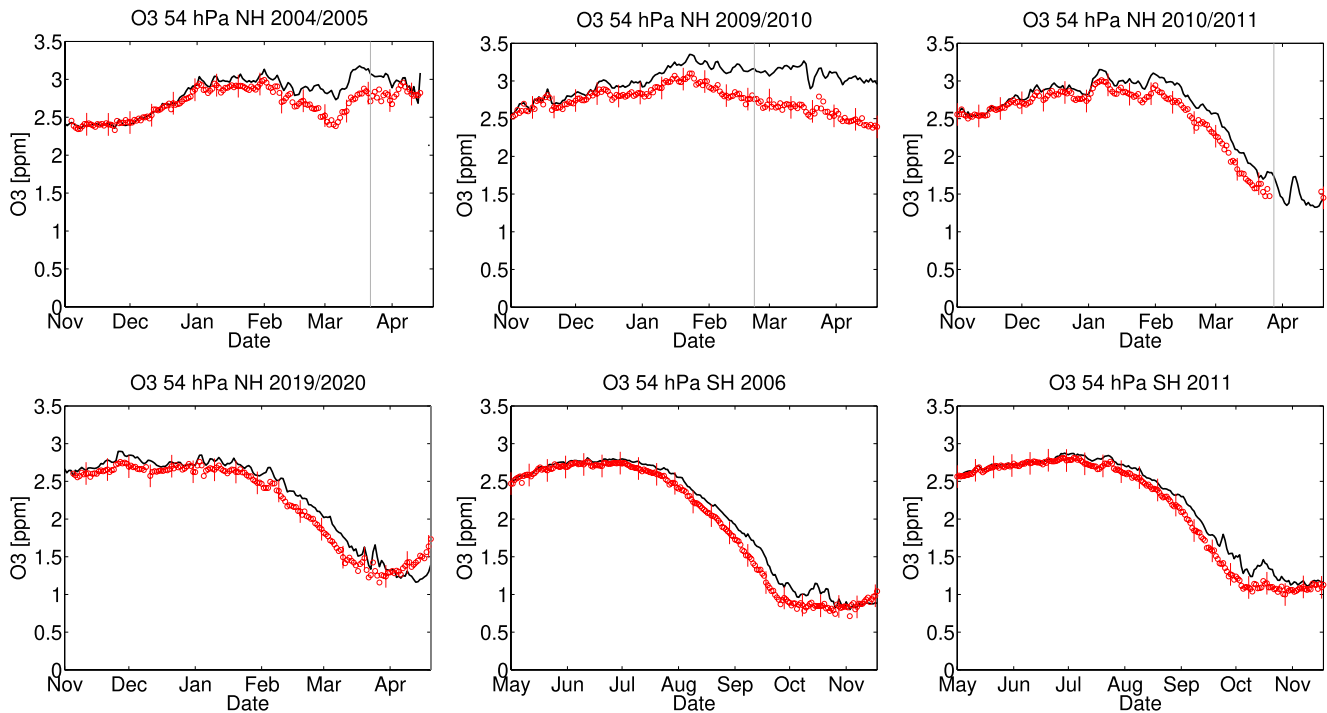


Figure 9. Modeled and observed ozone mixing ratios in the polar vortex at 54 hPa for the Arctic winters 2004/2005, 2009/2010, 2010/2011, and 2019/2020 and for the Antarctic winters 2006 and 2011. Modeled vortex averages (black) compared to corresponding vortex averages of the Microwave Limb Sounder instrument (red, bars show the accuracy of the measurements). The gray line shows the approximate breakup date of the Arctic polar vortex (see Section 5).

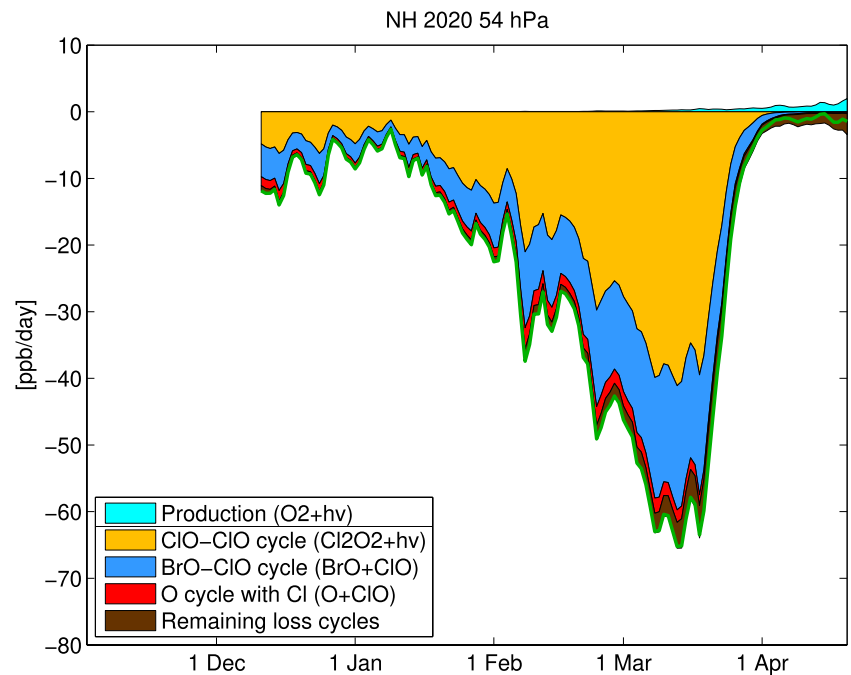


Figure 10. Chemical ozone depletion rates in the polar vortex core at 54 hPa for the Arctic winter 2019/2020. The green line shows the net chemical change rate of ozone, which nearly equals the change rate of odd oxygen at this altitude. The contribution of different catalytic cycles to the ozone loss is shown by the reaction rates of their rate-limiting step. Only the three most important cycles are shown. Ozone production is shown in cyan.

Figure 10 shows the chemical ozone depletion rates in the vortex core at 54 hPa for the winter 2019/2020 and the contribution of the different catalytic ozone depletion cycles. Ozone depletion can be divided into two phases: In December, a moderate depletion of about 10 ppb/day was observed. After a minimum at the start of January due to a lack of sunlight, depletion began to increase steadily from values near zero to depletion rates of up to 70 ppb/day in March. This increase is caused by the increase in sunlight, since temperatures were consistently low enough for chlorine activation in this time period. Ozone depletion ended quite abruptly at the end of March with the rise of temperatures. An increase in ozone depletion rates can also be caused by an increase in ClO_x by transport during the winter, but 2019/2020 showed a stable and cold vortex with weak transport (e.g., Lawrence et al., 2020) and relatively constant ClO_x values (Figure 3b).

The ClO-ClO cycle contributes about 60% to the ozone loss, while the ClO-BrO cycle contributes about 30%. This is comparable to values found in other studies (e.g., Frieler et al., 2006; Kuttippurath et al., 2010; Wohltmann et al., 2017). Again, figures corresponding to Figure 10 for additional years, for the northern and Southern Hemisphere, and for different altitude levels can be found in Wohltmann et al. (2017) (e.g., their Figure 20a, and supplement).

Figure 11 shows the chemical ozone depletion rates in the vortex at 54 hPa for different winters. Ozone depletion rates are generally higher in the vortex core than in the complete vortex (up to 70 ppb/day compared to 50 ppb/day). Significant ozone depletion in 2019/2020 (more than 5 ppb/day) is first observed at the beginning of December, which is unusually early (Manney et al., 2020), and lasts until the end of March. The high ozone depletion rates in December are caused by record low temperatures in November and early December in 2019 (Lawrence et al., 2020; Wohltmann et al., 2020). Ozone depletion rates for the Antarctic winters and the cold Arctic winters 2010/2011 and 2019/2020 are of comparable magnitude in most of the considered time period. While ozone depletion rates for the average winters 2004/2005 and 2009/2010 are similar to the rates of the other years in early winter, they are considerably lower in late winter compared to the cold Arctic and Antarctic winters (mainly because of the earlier breakdown of the vortex and the preceding temperature increase). The similar ozone depletion rates for Arctic and Antarctic winters may seem surprising at first sight. There are several points to note here:

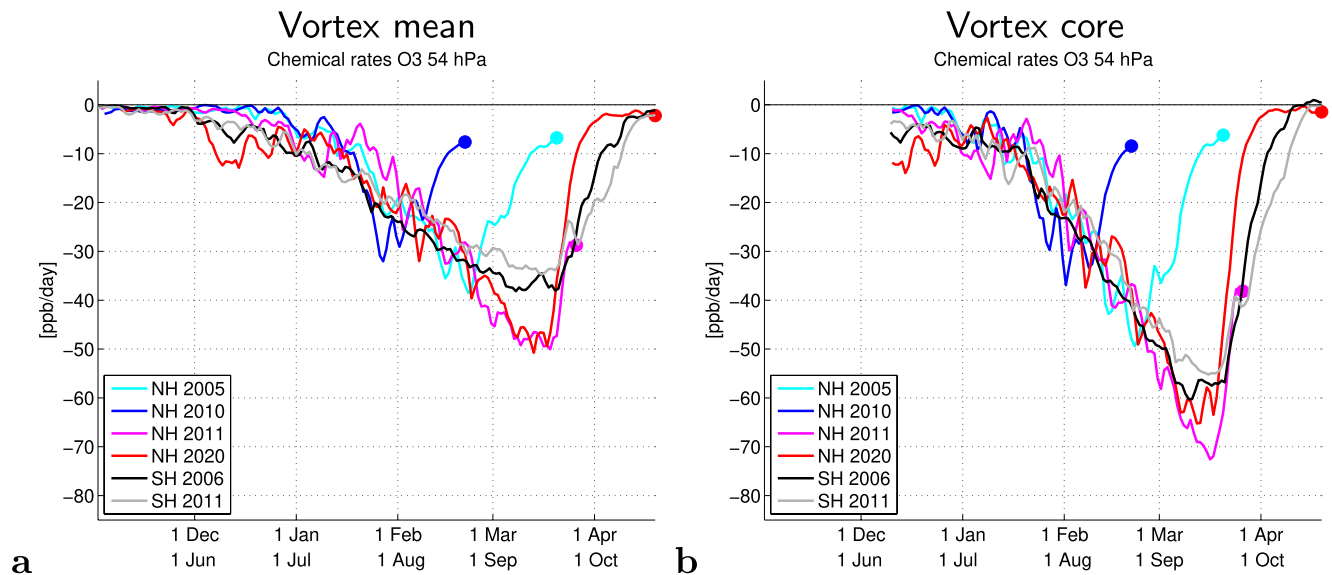


Figure 11. Chemical rate of change of ozone in the polar vortex at 54 hPa for the Arctic winters 2004/2005, 2009/2010, 2010/2011, and 2019/2020 and for the Antarctic winters 2006 and 2011. (a) Vortex means and (b) Means over the polar vortex core. Dots show the approximate breakup date of the Arctic polar vortex (see Section 5).

1. There is a good agreement between the modeled and observed ozone mixing ratios (Figure 9). This supports the validity of the modeled ozone loss rates, unless there are competing transport effects that lead to discrepancies. The difference between modeled and observed ozone in the Southern Hemisphere and in the cold Arctic winters is in fact smaller than in the warmer Arctic winters.
2. The vertical range where ozone depletion leads to very low mixing ratios (<0.2 ppm) is much larger in the Southern Hemisphere (about 350–510 K, e.g., Kuttippurath et al., 2018; Solomon et al., 2014) compared to the Arctic winter 2019/2020 (425–485 K, Wohltmann et al., 2020). This leads to much larger ozone loss in the total column in the Southern Hemisphere.
3. Our model may underestimate the ozone depletion rates in the Southern Hemisphere because of the difficulties in modeling HCl correctly (Figure 5). There is, however, evidence that the discrepancy in HCl does not translate to as large a discrepancy in ozone depletion rates. Modeled ClO and observed ClO agree better than expected from the discrepancy in HCl. Typically, the local underestimation of modeled ClO values compared to MLS is 0.2–0.4 ppb for peak values measured in sunlight (not shown). Assuming a partitioning of 70% for ClO in ClO_x (Wohltmann et al., 2017), this translates to an underestimation of ClO_x of 0.3–0.6 ppb. This is less than the observed differences in HCl of up to 1 ppb. The effect of the empirical correction of the HCl discrepancy in the model on ozone loss is small and on the order of magnitude of a few 0.1 ppm at 54 hPa (Groß et al., 2018; Wohltmann et al., 2017).

When trying to correct for the HCl discrepancy, there were several options (see Wohltmann et al., 2017). We chose to change the HCl solubility for the particular reason that while HCl does not agree well with measurements, ozone and ClO_x seem to be less affected. Our empirical correction hides HCl inside the PSCs and HCl in PSCs will not be observed by instruments that measure gas-phase HCl. At the same time, it does not significantly change the rest of the chemistry in the model.

4. In most Arctic winters of the last decades, the period of significant ozone loss (at most several weeks) was much shorter than in the Southern Hemisphere (typically more than 2 months).

Remarkably, the last point is not true for the Arctic winters 2010/2011 and 2019/2020 at 54 hPa. These winters show periods of significant ozone depletion that are comparable in length to those in the Southern Hemisphere and also show a similar magnitude of chemical ozone depletion rates.

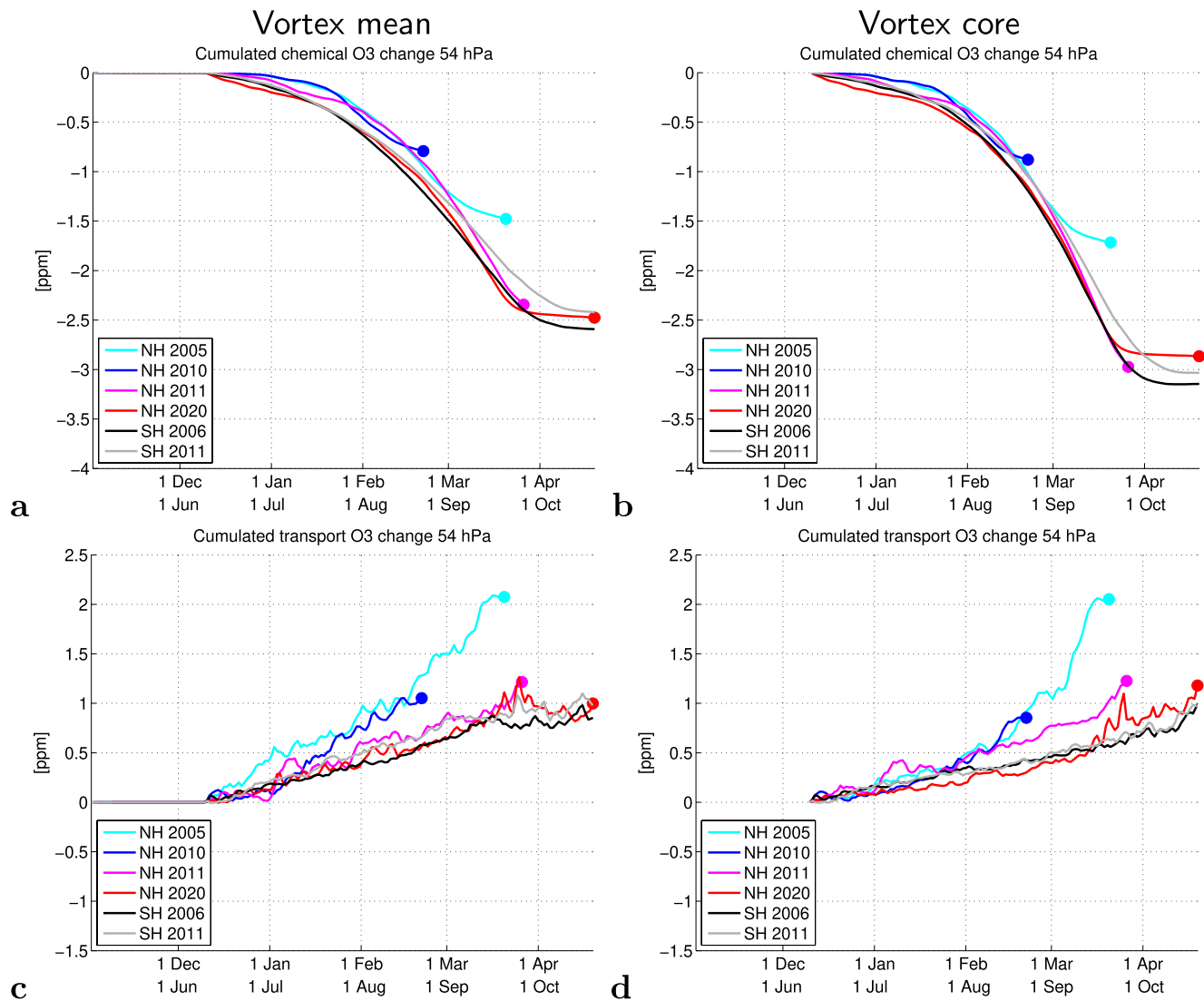


Figure 12. Accumulated change of ozone mixing ratio due to chemistry and due to transport in the polar vortex at 54 hPa for the Arctic winters 2004/2005, 2009/2010, 2010/2011, and 2019/2020 and for the Antarctic winters 2006 and 2011. (a, b) The accumulated chemical ozone change (integral of Figures 11a and 11b). (c, d) The same for accumulated ozone change due to transport (same vertical scale, but vertical axis shifted). (a, c) Vortex means and (b, d) Means over the polar vortex core. Antarctic values are shifted by half a year. Dots show the approximate breakup date of the Arctic polar vortex (see Section 5).

5.4. Ozone Changes by Transport Versus Ozone Changes by Chemistry

The evolution of the ozone mixing ratios is not only determined by ozone loss. Changes by transport and chemistry both contribute to the overall change. Changes by transport are more important in the Northern Hemisphere, where they contribute about equally to the interannual variability in polar ozone (e.g., Tegtmeier et al., 2008). Typically, a cold and stable vortex is associated with decreased downwelling, less mixing across the vortex edge, a weaker Brewer-Dobson circulation, a later vortex breakup and lower ozone (e.g., Newman et al., 2001; Randel et al., 2002; Tegtmeier et al., 2008), and the opposite for a warm and disturbed vortex. We will now have a closer look at the chemical and transport contributions to the overall change.

Figures 12a and 12b show the accumulated chemical change from Figure 11 (i.e., the integral over the curves), with a common start date of December 10 or June 10 (initialization dates of the vortex tracer). Figures 12c and 12d show the same for the accumulated change due to transport. The accumulated change due to transport is calculated as the difference between the accumulated total simulated change of ozone and the accumulated 44 hPa chemical change. The accumulated chemical change at 54 hPa is not identical to the

overall chemical loss experienced by a given air mass, since 54 hPa is not a material surface and we look at different air masses at different points of time. In all years, the chemical ozone loss is masked by transport of ozone from above and across the vortex edge. In warm years, this can lead to an increase in ozone, even though there is ozone loss (see Figure 8), while in colder years, the simulated change is somewhat less than expected from ozone depletion alone.

For the cold Arctic winters and the Antarctic winters, the vortex-averaged accumulated chemical loss is remarkably similar and amounts to about 2.3–2.6 ppm at the end of winter (defined as vortex breakup in the Northern Hemisphere and October 20 in the Southern Hemisphere; Figure 12a). In the vortex core, the corresponding values are 2.9–3.1 ppm (Figure 12b). The average Arctic winters 2004/2005 and 2009/2010 show lower vortex-averaged values of about 1.5 and 0.8 ppm, respectively (Figure 12a). The smaller loss at the end of winter for the average Arctic winters is mainly caused by the earlier breakup of the vortex and the shorter time period of ozone loss (and not so much by differences in loss rates).

The change by chemistry is partially offset by the accumulated change by transport at the end of the winter. The vortex-averaged rate of change by transport at a given point in time is larger for the average Arctic winters 2004/2005 and 2009/2010 than for the other winters, as expected from the larger downwelling by the Brewer–Dobson circulation in warm winters (Figure 12c). The Antarctic winters and the cold Arctic winters 2010/2011 and 2019/2020 show similar rates of change by transport (Figure 12c) and a similar vortex-averaged accumulated change by transport of 0.9–1.2 ppm at the end of winter. It has already been noted that the Arctic winter 2010/2011 was characterized by an exceptionally low contribution of transport and mixing to the ozone change (e.g., Balis et al., 2011; Lawrence et al., 2020; Strahan et al., 2013), and the Arctic winter 2019/2020 was very similar to 2010/2011 in this respect.

The higher rate of ozone change by transport in warm winters is partially compensated by a shorter time of change due to an earlier vortex breakup. The warm Arctic winter 2009/2010 shows an accumulated ozone change due to transport of 1.1 ppm at the end of the winter, that is similar to the corresponding value in cold winters (Figure 12c) because of these compensating effects. An exception for the years considered in this study is the Arctic winter 2004/2005, which shows a vortex-averaged change by transport of 2.1 ppm. The winter 2004/2005 was remarkable for having a weak polar vortex and unusually large mixing (e.g., Manney et al., 2006; Schoeberl et al., 2006). Moreover, the vortex breakup date is later in 2004/2005 than in 2009/2010.

In the vortex core, the winters 2010/2011 and 2019/2020 show a slightly higher positive accumulated change by transport than the Antarctic winters at the end of the winter (Figure 12d). This is caused by higher rates of change by transport in some parts of the considered time period. The accumulated negative change by chemistry for cold Arctic winters is similar or slightly lower compared to the Antarctic at the end of winter (Figure 8b). Taken together, this leads to higher simulated mixing ratios in the vortex core for the cold Arctic winters compared to Antarctic winters at the end of the winter (Figure 8b). In addition to the earlier vortex breakup, higher ozone mixing ratios at the start of December also play a role for the higher values in the Arctic winter 2010/2011 compared to 2019/2020 (Figure 8b). The higher mixing ratios are partly caused by the early ozone loss in December in 2019/2020, which was not evident in 2010/2011.

5.5. Ozone Loss Estimates in the Same Air Mass

The quantitative estimation of ozone loss in the same air mass (as opposed to the accumulated loss in different air masses at a given pressure level discussed so far) in the winter 2019/2020 is covered in detail elsewhere (e.g., Feng et al., 2021; Grooß & Müller, 2021; Manney et al., 2020; Wohltmann et al., 2020), and we will only give a short comparison of our results to other studies. The maximum in the simulated ozone loss profile averaged over the vortex obtained with a passive ozone tracer (see Wohltmann et al., 2020) is 2.3 ppm at about 450 K on April 1. The corresponding value for the vortex core is 2.7 ppm. The vortex-averaged partial column loss (370–550 K) is 123 DU on April 1. Grooß and Müller (2021) report values for the CLaMS model of 2.74 ppm in the vortex north of 75° equivalent latitude on March 30 and 131 DU partial column loss (370–550 K) north of 75° on April 4. Wohltmann et al. (2020) compare the ATLAS passive tracer to sondes and obtain an ozone loss of 2.8 ppm for sondes showing less than 0.2 ppm in the most depleted part of the vortex (March 23 to April 10) with a corresponding partial column loss of 124 DU (370–550 K).

Manney et al. (2020) give a value of 2.8 ppm for the MLS match approach and a vortex-averaged descent approach. Feng et al. (2021) give a value of 108 DU for the maximum ozone loss in the vortex total column on March 18 from the SLIMCAT model. This is lower than the other estimates but may miss some loss after March 18.

6. The Depleted Layer Observed in 2020

Observations of ozone sondes and satellites show a layer of highly depleted ozone centered around 450 K potential temperature in about 20% of the polar vortex area in March and April 2020 (Wohltmann et al., 2020). Typically, mixing ratios below 0.2 ppm were observed, with individual measurements showing values as low as 0.13 ppm (Wohltmann et al., 2020). Such a pronounced minimum in the vertical profile has never been observed in the Arctic before, with lowest observed ozone mixing ratios in any previous winter not lower than 0.5 ppm in 2011 (e.g., Solomon et al., 2014; Wohltmann et al., 2020). A detailed account of these observations and the associated ozone loss is given in Manney et al. (2020) and Wohltmann et al. (2020). Here, we take an additional look at the depleted layer from the perspective of the ATLAS model.

We use the same set of 52 ozone sonde profiles measured inside the polar vortex from March 17 to April 17, 2020 as in Wohltmann et al. (2020). Figure 13 shows examples of simulated and measured ozone sonde profiles. ATLAS is able to reproduce the shape and magnitude of the ozone minima in the sonde measurements, which confirms that the minima can be reproduced with our current understanding of ozone chemistry. Figure 13 indicates that significant ozone loss is observed between 370 and 550 K (difference between the black and red lines).

6.1. More Time Spent at Low Temperatures and in Sunlight Leads to More Ozone Depletion

For a better qualitative understanding of the mechanisms leading to this minimum, we examine the history of the air masses measured at the sonde locations. Ozone loss has two basic requirements: The first is temperatures below the upper temperature limit for the formation of polar stratospheric clouds, so that active chlorine is set free from chlorine reservoir gases. The second requirement is sunlight, which is needed for the catalytic photochemical ozone depletion cycles. Once there is sunlight, low temperatures are also required to stop active chlorine from being deactivated. Under these conditions, both activation and deactivation reactions proceed and chlorine remains activated, see discussion in Section 5.1, or for example, Portmann et al. (1996) and Solomon et al. (2015). In order to quantify the occurrence of PSCs and sunlight, we calculated backward trajectories from the position and time of the ozone soundings. For each trajectory, we determined the accumulated length of the time periods in which the corresponding air masses had not only been below the upper temperature limit for the formation of polar stratospheric clouds composed of NAT, but also in sunlight. In the following, we will call this quantity $\Delta t_{\text{psc+sun}}$. This approach was inspired by a similar approach for the relationship between PSC volume in the vortex and overall ozone loss (e.g., Rex et al., 2004, 2006), which is refined by taking sunlight into account in some studies (e.g., Pommereau et al., 2018).

6.2. Calculation of $\Delta t_{\text{psc+sun}}$

We start backward trajectories from the location and time of the sonde measurements from 370 to 550 K in 1 K steps to calculate $\Delta t_{\text{psc+sun}}$. The trajectories are run backward for 4 months with a 10 min time step and are calculated with the trajectory module of the ATLAS model. The model uses meteorological data and diabatic heating rates from ERA5 to calculate the vertical motion. The upper temperature limit T_{NAT} for the formation of NAT clouds is calculated as in Hanson and Mauersberger (1988) along the trajectories. Mixing ratios of HNO_3 are taken from measured MLS profiles closest to the trajectory location on the day of the respective trajectory time step. All 10 min time periods that show a temperature below T_{NAT} and a solar zenith angle below 90° are summed for each individual trajectory. Trajectories that spent a significant time far outside the polar vortex are discarded. This is accomplished by rejecting any trajectories that show a modified potential vorticity smaller than 25 PVU at any point in time.

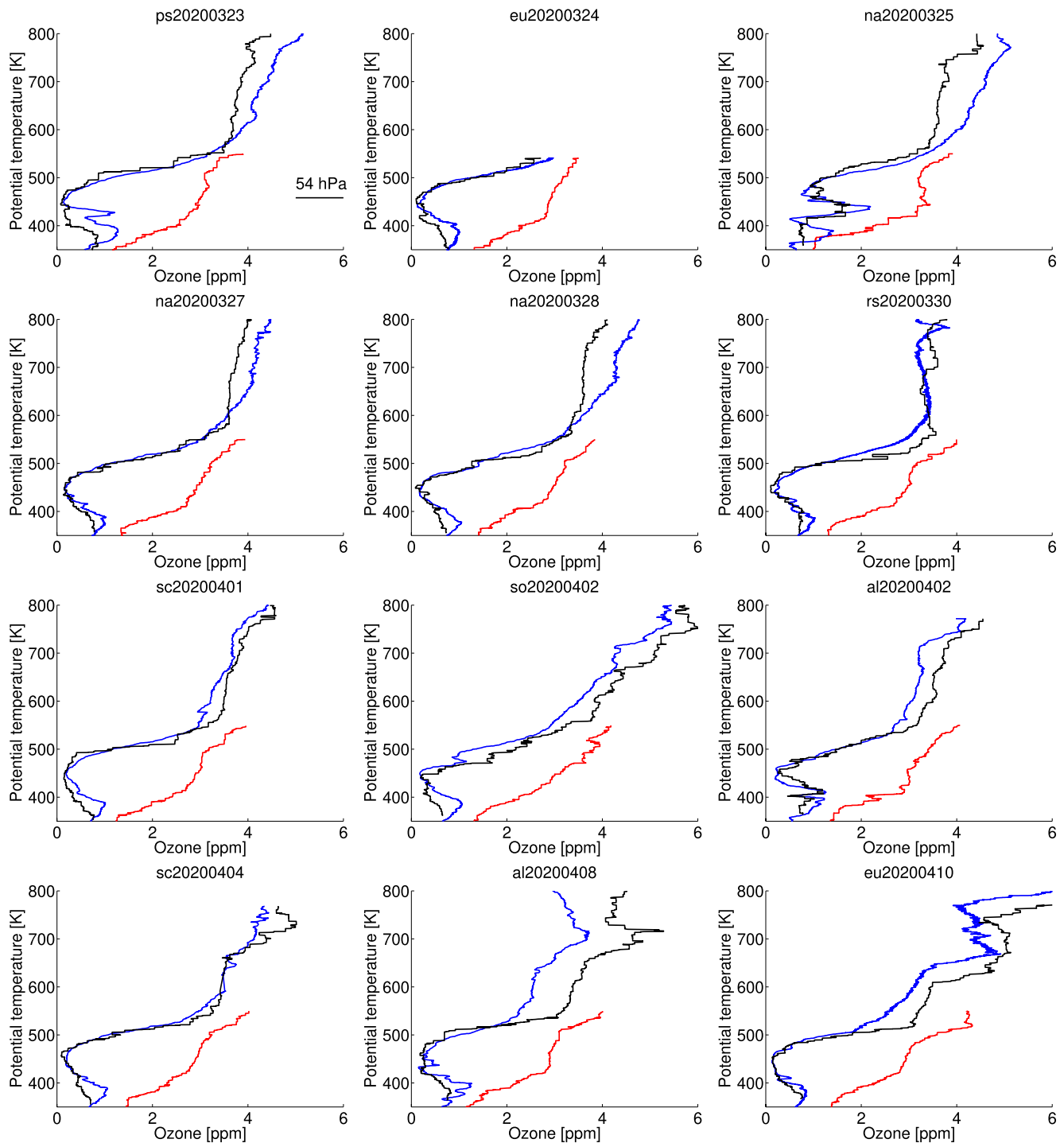


Figure 13. Examples of ozone sonde profiles measured at end of March and beginning of April 2020, as a function of potential temperature. Blue lines show individual ozone sonde measurements. Black lines show the simulated ozone of the ATLAS model interpolated to the position of the sonde measurement. Red lines show a passive ozone tracer from the ATLAS model interpolated to the position of the sonde measurement. Values for the passive ozone tracer are only reliable below 550 K (Wohlmann et al., 2020). The difference between the passive tracer and ozone is the chemical ozone loss. The 54 hPa level is indicated (first subplot). Profiles were measured at Alert (al, 82.5°N, 62.3°W), Eureka (eu, 80.0°N, 85.9°W), Ittoqortoormiit (Scoresbysund; sc, 70.5°N, 22.0°W), Ny-Ålesund (na, 78.9°N, 11.9°E), Resolute (rs, 74.7°N, 94.9°W), and Sodankylä (so, 67.4°N, 26.6°E) and above the Polarstern vessel in the Arctic Ocean (ps, 86.2°N, 15.8°E) during the MOSAiC expedition (von der Gathen & Maturilli, 2020).

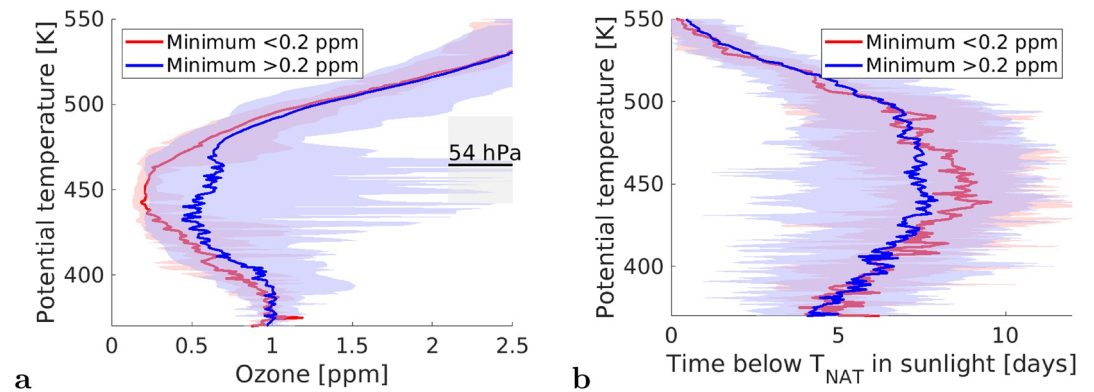


Figure 14. (a) Ozone sonde profiles inside the polar vortex averaged from March 17 to April 17, 2020. The red line is the average of all sondes with a minimum mixing ratio below 0.2 ppm; the blue line shows the average of all other sondes. Shading shows minimum and maximum values. The mean position of the 54 hPa level is indicated. Shading shows minimum and maximum values. (b) Average of the length of the accumulated time periods spent below the upper temperature limit for the formation of NAT clouds (T_{NAT}) and in sunlight for the air masses measured by the sondes. Shading shows minimum and maximum values.

6.3. Linear Relation of Ozone Loss and $\Delta t_{\text{psc+sun}}$

To a first-order approximation, the relation between $\Delta t_{\text{psc+sun}}$ and the accumulated ozone loss is linear. Ozone is depleted by the catalytic ClO-ClO and ClO-BrO cycles (Figure 10). The rates of these catalytic loss cycles are not dependent on the ozone mixing ratio. That means, that as long as ClO_x is approximately constant, ozone is depleted with an approximately constant rate. Assuming that all available chlorine is fully activated into ClO_x when PSCs are present and when there is sunlight, and that it is quickly deactivated or that there is no ozone loss after the disappearance of PSCs or when there is a lack of sunlight, leads to a linear relationship between $\Delta t_{\text{psc+sun}}$ and the accumulated ozone loss. Notably, the detailed reaction pathways for activation (e.g., by $\text{ClONO}_2 + \text{HCl}$ or $\text{HOCl} + \text{HCl}$) or deactivation (e.g., by $\text{Cl} + \text{CH}_4$ or $\text{ClO} + \text{NO}_2$) are not relevant for this relationship. However, chlorine activation during the time covered by $\Delta t_{\text{psc+sun}}$ may stop if one of the chlorine reservoir gases is depleted (and cannot be regenerated or substituted by another reaction partner fast enough).

6.4. Minimum Ozone Mixing Ratios

Typical observed minimum mixing ratios in the ozone hole in the Antarctic vortex are about 0.01–0.1 ppm, which approaches the detection limit of ozone sondes and satellite instruments (e.g., Solomon et al., 2014; Wohltmann et al., 2020). Lowest observed values in the Arctic winter 2020 are about 0.1–0.2 ppm. Taking this together, we define 0.05 ppm as a reasonable threshold value for “near zero ozone” in the following.

6.5. Results

Figure 14a shows the average of all sonde measurements with a minimum mixing ratio below 0.2 ppm from March 17 to April 17, 2020 in red. The average of all other sonde measurements in this time period is shown in blue. Figure 14b shows the corresponding averages of $\Delta t_{\text{psc+sun}}$ for the air masses measured by the sondes. The average of the sondes partly accounts for the “butterfly” effect, where small differences in the initial conditions of the trajectories can grow exponentially, and tends to cancel out the uncertainties caused by this. The basic assumption made is that while the results for individual trajectories will be meaningless for longer time periods, the result for the average will be a suitable approximation. The results for adjacent potential temperature levels also give an indication of these uncertainties.

Figures 13 and 14 indicate that the vertical extent of the ozone minimum and of ozone depletion correlates well with $\Delta t_{\text{psc+sun}}$ along the backward trajectories. Higher values of $\Delta t_{\text{psc+sun}}$ are typically correlated with

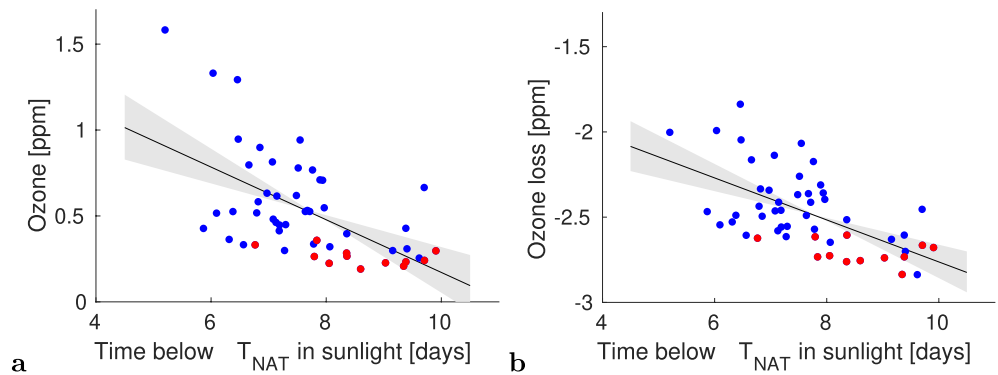


Figure 15. (a) Ozone mixing ratio measured by individual sondes averaged over 430–470 K versus the corresponding average of the accumulated time spent below the upper temperature limit for the formation of NAT clouds in sunlight for the air masses measured by the sondes. Shading shows uncertainty for the regression line (95% confidence interval obtained from a bootstrap approach by resampling of the residuals). Sondes with a minimum mixing ratio below 0.2 ppm are shown in red. (b) Same, but showing ozone loss instead of ozone mixing ratios. Ozone loss is determined as the difference between the sonde measurements and a passive ozone tracer from the ATLAS run interpolated to the locations of the sondes.

lower ozone mixing ratios and more ozone loss. The vertical range of ozone depletion is limited by the temperature profile of the stratosphere in combination with the strong altitude dependence of T_{NAT} .

The sondes with a minimum below 0.2 ppm show mixing ratios that are on average 0.3–0.4 ppm lower than the mixing ratios of the other sondes. At the same time, the air parcels measured by these sondes spent about 28 h more time below T_{NAT} and in sunlight than the other sondes (mean over 430–470 K). This suggests that the lowest observed mixing ratios were caused by exceptionally long periods with low temperatures in sunlight in the history of these air masses.

Figure 15a shows that the relation between $\Delta t_{\text{psc+sun}}$ and measured ozone also holds for individual sondes in a statistical sense. The figure shows a scatter plot of the ozone mixing ratio of individual sondes averaged over 430–470 K and the corresponding averages of $\Delta t_{\text{psc+sun}}$ for the air masses measured by the sondes. The 430–470 K range is a compromise between reducing the uncertainty in Figure 15 and a sufficiently small vertical range. A change in measured ozone of 153 ± 58 ppb per 24 h spent below T_{NAT} and in sunlight can be deduced from the slope of a regression line fitted through the points in Figure 15a. Uncertainty limits represent the 95% confidence interval obtained from the distribution of the fitted slopes in a bootstrap approach by resampling of the residuals.

However, the slope of the regression line through the observed ozone mixing ratios is no direct measure of the relation of ozone loss and $\Delta t_{\text{psc+sun}}$; the observed ozone mixing ratios depend not only on ozone loss but also on the initial ozone mixing ratios at the onset of ozone loss and on mixing processes. The latter two may correlate with the position of the air parcels in the vortex and thus also with $\Delta t_{\text{psc+sun}}$. For this reason, Figure 15b shows the corresponding relation between $\Delta t_{\text{psc+sun}}$ and ozone loss. Ozone loss is determined as the difference in mixing ratios between the sonde measurements and a passive ozone tracer from the ATLAS run interpolated to the locations of the sondes and initialized on December 10 (see Wohltmann et al., 2020). Note that Figure 15a is solely based on measurements, while ozone loss is also based on model results. A chemical ozone loss rate of 123 ± 44 ppb per 24 h spent below T_{NAT} and in sunlight can be deduced from the slope of a regression line fitted through the points in Figure 15b (not to be confused with the ozone loss rate per calendar day, which is e.g., shown in Figure 11). This means that only an additional 21–46 h below T_{NAT} and in sunlight would have been necessary to reduce ozone from 0.2 ppm to near zero values (0.05 ppm) based on a simple extrapolation of the loss rates.

6.6. Discussion

There is some subjectivity in choosing an initial mixing ratio from where the calculation of the additional loss for the simple extrapolation (Figure 15b) should start, but it seems reasonable to use the value of

0.2 ppm stated earlier for the approximate minimum values in about 20% of the vortex, since we are interested in the question when ozone is depleted to near zero values in the most depleted part of the vortex. Additionally, we assume for simplicity that the linear relationship between ozone loss and $\Delta t_{\text{psc}+\text{sun}}$ is maintained when ozone decreases and holds for all ozone values greater than zero. Under these assumptions, 21–46 h below T_{NAT} and in sunlight are needed to decrease ozone to 0.05 ppm when using the uncertainty limits for the slope from above.

The ozone sonde measurements used in Figure 14 were performed during a period of 4 weeks. As ozone declines and $\Delta t_{\text{psc}+\text{sun}}$ increases (or stays constant) with time, spurious effects in Figure 14 could arise if the time sampling of the sonde measurements with ozone below 0.2 ppm was different from the time sampling of the sonde measurements with ozone above 0.2 ppm. However, temperatures were too high for the formation of polar stratospheric clouds after end of March, so that contributions to $\Delta t_{\text{psc}+\text{sun}}$ (and also to ozone loss) arise from a time interval shorter than the 4 weeks mentioned above, which reduces the opportunities for spurious effects.

A closer inspection of the correlation between $\Delta t_{\text{psc}+\text{sun}}$ and ozone loss shows that the correlation is mainly caused by the conditions after January 15. Figure 15 would look similar if rather than the full backward trajectories (which go back to beginning of December), only the parts after January 15 were used. This is mainly caused by the lack of sunlight before January 15 (see Figure 1, and see also the low ozone loss rates in Figure 10). This means that differences in the accumulated time periods below T_{NAT} before January 15 are not very relevant and that the accumulated time periods below T_{NAT} in late winter and spring are important, when both activation and deactivation reactions proceed (see Figure 4).

Using only the data after January 15 does also change the fitted slopes. The change in measured ozone increases to 196 ± 58 ppb per 24 h spent below T_{NAT} and in sunlight, and the chemical ozone loss rate increases to 150 ± 45 ppb per 24 h spent below T_{NAT} and in sunlight. With these values, 18–34 h below T_{NAT} and in sunlight are needed to decrease ozone to 0.05 ppm. These differences can be considered part of the systematic uncertainty of the approach. For the ozone loss, it seems to be more reasonable to use the complete time period and not only the time period after January 15 to calculate the ozone loss rates per 24 h spent below T_{NAT} and in sunlight, since the passive ozone tracer was initialized on December 10.

6.7. Example Trajectories

Figures 16a–16f show the meteorological conditions, the accumulated time periods in sunlight, and the accumulated time periods below T_{NAT} along two exemplary ensembles of backward trajectories. As an example for low ozone, we choose the sonde measurement of 0.16 ppm at 445 K in Ny-Ålesund on March 27, 2020, and as an example for high ozone, we choose the sonde measurement of 1.6 ppm at 445 K at the same location on March 25, 2020. In each case, nine ensemble trajectories were started from 441 to 449 K to account for uncertainty in trajectory evolution, where small differences in the initial conditions can cause trajectories to diverge exponentially. Figure 17 shows the measured ozone profiles (a) and the chemical evolution along the trajectories interpolated to the position of the trajectories from the results of the ATLAS run (b–f). The calculation of T_{NAT} for Figures 16d and 16f are based on the modeled values of HNO_3 (Figure 17c) and H_2O along the trajectories.

The potential vorticity along the trajectories in Figure 16a shows that the air measured on March 27 (low ozone) was located closer to the vortex core in the last 3 months before the measurement than the air measured on March 25 (high ozone). In turn, the trajectories with low ozone experienced lower temperatures (Figures 16b and 16d) and less sunlight (Figure 16e) than the trajectories with high ozone. This means two competing changes compared to the trajectories with high ozone: The accumulated time periods with a solar zenith angle below 90° are shorter (Figure 16e), but the accumulated time periods below T_{NAT} are longer (Figure 16d). The result for the $\Delta t_{\text{psc}+\text{sun}}$ metric is that it is smaller for the trajectories with low ozone until mid-February but that it is higher in March (Figure 16f).

These results are reflected in the evolution of the mixing ratios of key species along the trajectories in the ATLAS model (Figures 17b–17f). The figures show the daily average over all ATLAS air parcels within 250 km horizontal distance and 20 K vertical distance of the current trajectory locations (first calculated

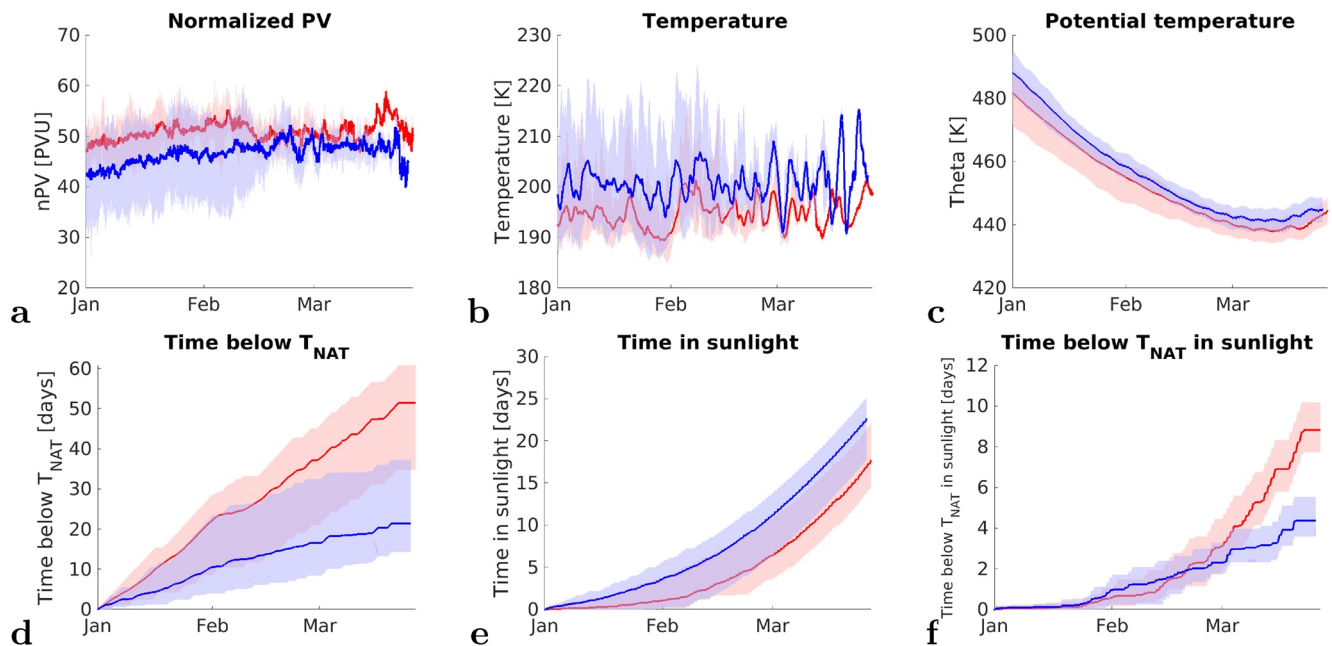


Figure 16. Meteorological conditions, accumulated time periods of sunlight, and accumulated time periods below T_{NAT} along two ensembles of exemplary backward trajectories. As an example for high ozone, we choose the sonde measurement of 1.6 ppm at 445 K at Ny-Ålesund on March 25, 2020 (blue). Nine ensemble trajectories were started from 441 to 449 K to account for uncertainties in trajectory evolution. As an example for low ozone, we choose the sonde measurement of 0.16 ppm at 445 K at Ny-Ålesund on March 27, 2020 (red). The panels show time series along the trajectories for (a) Modified potential vorticity, (b) Temperature, (c) Potential temperature, (d) Accumulated time period below T_{NAT} , (e) Accumulated time periods in sunlight, and (f) Accumulated time periods below T_{NAT} and in sunlight. The lines are the ensemble mean; the shading shows minimum and maximum values.

for each of the nine trajectories individually, and then mean, minimum, and maximum were applied). The evolution of ozone is relatively similar until the end of February, when values around 1.5 ppm are reached, but after this date values for the trajectories with low ozone start to fall to values around 0.2 ppm, while the trajectories with high ozone stay at approximately constant values (Figure 17b). The trajectories with low ozone start under more denitrified conditions because of the lower temperatures (Figure 17c). This impedes deactivation into ClONO_2 (Figure 17f). In fact, one of the most striking differences between the trajectories is that the trajectories with low ozone show deactivation into HCl (Figure 17e), while the trajectories with high ozone show deactivation into ClONO_2 (Figure 17f). The differences between the trajectories are also apparent in the mixing ratios of ClO_x (Figure 17d), which show significantly higher values for the trajectories with low ozone in February and March.

7. Conclusions

The winter 2019/2020 showed the lowest ozone mixing ratios ever observed in the Arctic winter stratosphere and was characterized by an unusually strong, long-lasting, and cold polar vortex. We performed simulations with the ATLAS model to study the chemical evolution and ozone depletion in the winter 2019/2020. We compared the results to simulations of the Arctic winters 2004/2005, 2009/2010, and 2010/2011 and of the Antarctic winters 2006 and 2011 to assess whether the chemical evolution and chemical processes in 2019/2020 are more characteristic of typical conditions in Antarctic winters or in average Arctic winters. Our study puts an emphasis on polar vortex means and the 54 hPa pressure level to keep the discussion focused.

Results show that in some respects, the winter 2019/2020 (and also the winter 2010/2011) was a hybrid between Arctic and Antarctic conditions. While deactivation of active chlorine usually proceeds into ClONO_2 in the Northern Hemisphere and into HCl in the Southern Hemisphere, deactivation into both ClONO_2 and HCl was modeled in 2019/2020 and 2010/2011. Significant activation of chlorine via $\text{HOCl} + \text{HCl}$, which is

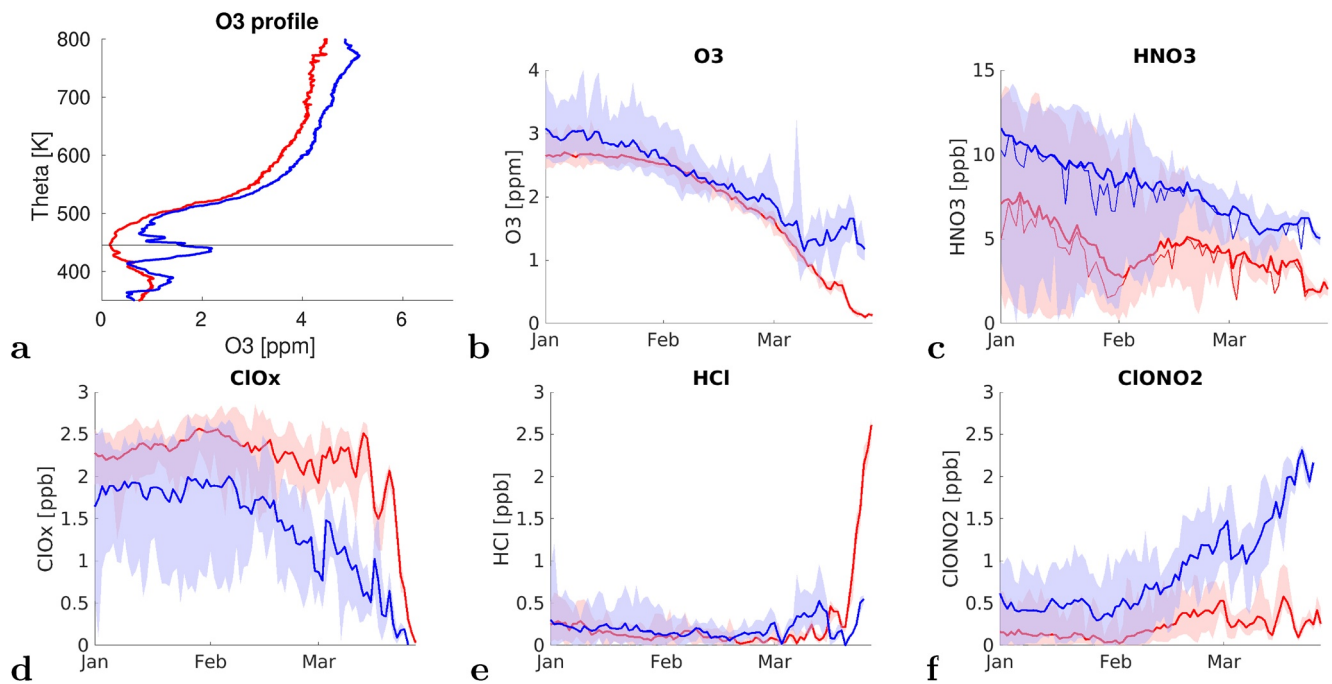


Figure 17. Chemical evolution along the two exemplary backward trajectory ensembles from Figure 16. (a) The measured ozone profiles in Ny-Ålesund on March 25, 2020 (blue) and March 27, 2020 (red). The starting altitude of the backward trajectories is marked by a black line. (b–f) Time series along the trajectories interpolated to the position of the trajectories from the results of the ATLAS run for (b) Ozone, (c) HNO₃ (total, thick line, and gas-phase, thin line), (d) ClO_x, (e) HCl, and (f) ClONO₂. The lines are the ensemble mean, the shading shows minimum and maximum values.

usually only observed in the Antarctic, was simulated in 2019/2020 and 2010/2011. In addition, denitrification and HNO₃ mixing ratios were also between the values for average Arctic winters and Antarctic winters.

Vortex-averaged chemical ozone loss rates at 54 hPa in 2010/2011 and 2019/2020 were comparable to typical loss rates in the Antarctic. In addition, the time period of significant chemical ozone loss in 2010/2011 and 2019/2020 was comparable to that in the Antarctic, leading to a similar accumulated chemical loss at 54 hPa. Slightly higher modeled ozone mixing ratios in the vortex core in 2010/2011 and 2019/2020 than in the Antarctic winters were found to be caused by more dynamical resupply of ozone by the Brewer-Dobson circulation.

However, there remain considerable differences between the conditions in the Arctic and Antarctic, even for the winters 2010/2011 and 2019/2020. The vertical extent and the area of low ozone values (less than 0.2 ppm) in the Antarctic are much larger, there is more loss in the column, and the area of low column values (below 220 DU) inside the vortex is larger (e.g., Damers et al., 2021; Manney et al., 2020; Wohltmann et al., 2020). Observed local minimum values are an order of magnitude smaller in the Antarctic. This is related to the fact that temperatures in the Antarctic vortex are lower and that low temperatures cover a larger part of the vortex (e.g., Solomon et al., 2014), see also, for example, Figure 1 of Wohltmann et al. (2020).

In addition, we examined the causes for the pronounced ozone minimum of less than 0.2 ppm at about 450 K potential temperature that was observed by ozone sondes in about 20% of the vortex area in spring 2020 (Wohltmann et al., 2020). Backward trajectory calculations show that the lowest observed mixing ratios were caused by exceptionally long periods with low temperatures in sunlight in the history of these air masses. Chemical ozone loss rates of 123 ± 44 ppb per 24 h spent below the upper temperature limit for the formation of NAT clouds and in sunlight can be deduced from ozone sonde measurements and the history of the measured air masses. This is not to be confused with the ozone loss per calendar day. Only an additional 21–46 h below the upper temperature limit for the formation of NAT clouds and in sunlight would have been necessary to reduce ozone to near zero values (0.05 ppm) in these parts of the vortex based on a simple extrapolation of the observed loss rates.

Data Availability Statement

Ozone sonde data are available from the World Ozone and Ultraviolet Radiation Data Center (WOUDC) at <https://woudc.org> and the Network for the Detection of Atmospheric Composition Change (NDACC) at <https://www.ndacc.org>. Ozone sonde data from the MOSAiC expedition are available at <https://doi.org/10.1594/PANGAEA.919538>. MLS data are available at [https://disc.gsfc.nasa.gov/datasets?page=1&keywords=AURA MLS](https://disc.gsfc.nasa.gov/datasets?page=1&keywords=AURA%20MLS). ECMWF ERA5 data are available at <https://cds.climate.copernicus.eu/cdsapp#!/home>.

Acknowledgments

The authors are grateful to the operating staff of all participating stations for having made the ozone sonde campaign in 2019/2020 possible. The authors acknowledge the support of the International Multidisciplinary Drifting Observatory for the Study of the Arctic Climate (MOSAIC) project with the tag MOSAiC20192020 and the Project_Id AWI_PS122_00. The authors thank the MLS Science Team for producing and making public the version 4 MLS data. The authors thank ECMWF for providing ERA5 reanalysis data, generated using Copernicus Climate Change Service Information 2020. Neither the European Commission nor ECMWF is responsible for any use that may be made of the Copernicus Information or Data it contains. Copernicus Climate Change Service (C3S; 2017): ERA5: Fifth generation of ECMWF atmospheric reanalyses of the global climate. Copernicus Climate Change Service Climate Data Store (CDS), 2017–2020. Open access funding enabled and organized by Projekt DEAL.

References

- Balis, D., Isaksen, I. S. A., Zerefos, C., Zyrichidou, I., Eleftheratos, K., Tourpali, K., et al. (2011). Observed and modelled record ozone decline over the Arctic during winter/spring 2011. *Geophysical Research Letters*, *38*, L23801. <https://doi.org/10.1029/2011GL049259>
- Bednarz, E. M., Maycock, A. C., Abraham, N. L., Braesicke, P., Dessens, O., & Pyle, J. A. (2016). Future Arctic ozone recovery: The importance of chemistry and dynamics. *Atmospheric Chemistry and Physics*, *16*, 12159–12176. <https://doi.org/10.5194/acp-16-12159-2016>
- Brakebusch, M., Randall, C. E., Kinnison, D. E., Tilmes, S., Santee, M. L., & Manney, G. L. (2013). Evaluation of whole atmosphere community climate model simulations of ozone during arctic winter 2004–2005. *Journal of Geophysical Research: Atmospheres*, *118*, 2673–2688. <https://doi.org/10.1002/jgrd.50226>
- Burkholder, J. B., Sander, S. P., Abbatt, J., Barker, J. R., Cappa, C., Crouse, J. D., et al. (2019). *Chemical kinetics and photochemical data for use in atmospheric studies, evaluation number 19*. Jet Propulsion Laboratory, California Institute of Technology. Retrieved from <http://jpldataeval.jpl.nasa.gov>
- Butchart, N., Cionni, I., Eyring, V., Shepherd, T. G., Waugh, D. W., Akiyoshi, H., et al. (2010). Chemistry-climate model simulations of twenty-first century stratospheric climate and circulation changes. *Journal of Climate*, *23*, 5349–5374. <https://doi.org/10.1175/2010JCLI3404.1>
- Crutzen, P. J., Müller, R., Brühl, C., & Peter, T. (1992). On the potential importance of the gas phase reaction $\text{CH}_2\text{O}_2 + \text{ClO} \rightarrow \text{ClOO} + \text{CH}_3$ and the heterogeneous reaction $\text{HOCl} + \text{HCl} \rightarrow \text{H}_2\text{O} + \text{Cl}_2$ in “ozone hole” chemistry. *Geophysical Research Letters*, *19*(11), 1113–1116. <https://doi.org/10.1029/92GL01172>
- Dameris, M., Loyola, D. G., Nützel, M., Coldewey-Egbers, M., Lerot, C., Romahn, F., & van Roozendael, M. (2021). Record low ozone values over the arctic in boreal spring 2020. *Atmospheric Chemistry and Physics*, *21*, 617–633. <https://doi.org/10.5194/acp-21-617-2021>
- Dhomse, S., Kinnison, D., Chipperfield, M., Cionni, I., Hegglin, M., Abraham, N. L., et al. (2018). Estimates of ozone return dates from chemistry-climate model initiative simulations. *Atmospheric Chemistry and Physics*, *18*, 8409–8438. <https://doi.org/10.5194/acp-18-8409-2018>
- Dorf, M., Butz, A., Camy-Peyret, C., Chipperfield, M. P., Kritten, L., & Pfeilsticker, K. (2008). Bromine in the tropical troposphere and stratosphere as derived from balloon-borne BrO observations. *Atmospheric Chemistry and Physics*, *8*, 7265–7271. <https://doi.org/10.5194/acp-8-7265-2008>
- Douglass, A. R., Schoeberl, M. R., Stolarski, R. S., Waters, J. W., Russell, J. M., III, Roche, A. E., & Massie, S. T. (1995). Interhemispheric differences in springtime production of HCl and ClONO₂ in the polar vortices. *Journal of Geophysical Research*, *100*(D7), 13967–13978. <https://doi.org/10.1029/95JD00698>
- Farman, J. C., Gardiner, B. G., & Shanklin, J. D. (1985). Large losses of total ozone in Antarctica reveal seasonal ClO_x/NO_x interaction. *Nature*, *315*, 207–210. <https://doi.org/10.1038/315207a0>
- Feng, W., Dhomse, S. S., Arosio, C., Weber, M., Burrows, J. P., Santee, M. L., & Chipperfield, M. P. (2021). Arctic ozone depletion in 2019/20: Roles of chemistry, dynamics and the Montreal protocol. *Geophysical Research Letters*, *48*, e2020GL091911. <https://doi.org/10.1029/2020GL091911>
- Frieler, K., Rex, M., Salawitch, R. J., Canty, T., Streibel, M., Stimpfle, R. M., et al. (2006). Toward a better quantitative understanding of polar stratospheric ozone loss. *Geophysical Research Letters*, *33*, L10812. <https://doi.org/10.1029/2005GL025466>
- Grooß, J.-U., Brauttsch, K., Pommerich, R., Solomon, S., & Müller, R. (2011). Stratospheric ozone chemistry in the Antarctic: What determines the lowest ozone values reached and their recovery? *Atmospheric Chemistry and Physics*, *11*, 12217–12226. <https://doi.org/10.5194/acp-11-12217-2011>
- Grooß, J.-U., Günther, G., Konopka, P., Müller, R., McKenna, D. S., Stroth, F., et al. (2002). Simulation of ozone depletion in spring 2000 with the Chemical Lagrangian Model of the Stratosphere (CLaMS). *Journal of Geophysical Research*, *107*(D20), 8295. <https://doi.org/10.1029/2001JD000456>
- Grooß, J.-U., & Müller, R. (2021). Simulation of record Arctic stratospheric ozone depletion in 2020. *Journal of Geophysical Research: Atmospheres*, *126*, e2020JD033339. <https://doi.org/10.1029/2020JD033339>
- Grooß, J.-U., Müller, R., Spang, R., Tritscher, I., Wegner, T., Chipperfield, M. P., et al. (2018). On the discrepancy of HCl processing in the core of the wintertime polar vortices. *Atmospheric Chemistry and Physics*, *18*, 8647–8666. <https://doi.org/10.5194/acp-18-8647-2018>
- Hanson, D., & Mauersberger, K. (1988). Laboratory studies of the nitric acid trihydrate: Implications for the south polar stratosphere. *Geophysical Research Letters*, *15*(8), 855–858. <https://doi.org/10.1029/GL015i008p00855>
- Hersbach, H., Bell, B., Berrisford, P., Hirahara, S., Horányi, A., Muñoz-Sabater, J., et al. (2020). The ERA5 global reanalysis. *Quarterly Journal of the Royal Meteorological Society*, *146*, 1999–2049. <https://doi.org/10.1002/qj.3803>
- Ivy, D. J., Solomon, S., & Thompson, D. W. J. (2014). On the identification of the downward propagation of Arctic stratospheric climate change over recent decades. *Journal of Climate*, *27*, 2789–2799. <https://doi.org/10.1175/JCLI-D-13-00445.1>
- Koo, J.-H., Walker, K. A., Jones, A., Sheese, P. E., Boone, C. D., Bernath, P. F., & Manney, G. L. (2017). Global climatology based on the ACE-FTS version 3.5 dataset: Addition of mesospheric levels and carbon-containing species in the UTLS. *Journal of Quantitative Spectroscopy and Radiative Transfer*, *186*, 52–62. <https://doi.org/10.1016/j.jqsrt.2016.07.003>
- Kuttippurath, J., Godin-Beekmann, S., Lefèvre, F., & Goutail, F. (2010). Spatial, temporal, and vertical variability of polar stratospheric ozone loss in the Arctic winters 2004/2005–2009/2010. *Atmospheric Chemistry and Physics*, *10*, 9915–9930. <https://doi.org/10.5194/acp-10-9915-2010>
- Kuttippurath, J., Kumar, P., Nair, P. J., & Pandey, P. C. (2018). Emergence of ozone recovery evidenced by reduction in the occurrence of Antarctic ozone loss saturation. *npj Climate and Atmospheric Science*, *1*, 42. <https://doi.org/10.1038/s41612-018-0052-6>
- Lait, L. R. (1994). An alternative form for potential vorticity. *Journal of the Atmospheric Sciences*, *51*(12), 1754–1759. [https://doi.org/10.1175/1520-0469\(1994\)051<1754:AAFFPV>2.0.CO;2](https://doi.org/10.1175/1520-0469(1994)051<1754:AAFFPV>2.0.CO;2)

- Langematz, U., Meul, S., Grunow, K., Romanowsky, E., Oberländer, S., Abalichin, J., & Kubin, A. (2014). Future Arctic temperature and ozone: The role of stratospheric composition changes. *Journal of Geophysical Research: Atmospheres*, *119*, 2092–2112. <https://doi.org/10.1002/2013JD021100>
- Lawrence, Z. D., Manney, G. L., & Wargan, K. (2018). Reanalysis intercomparisons of stratospheric polar processing diagnostics. *Atmospheric Chemistry and Physics*, *18*, 13547–13579. <https://doi.org/10.5194/acp-18-13547-2018>
- Lawrence, Z. D., Perlwitz, J., Butler, A. H., Manney, G. L., Newman, P. A., Lee, S. H., & Nash, E. R. (2020). The remarkably strong Arctic stratospheric polar vortex of winter 2020: Links to record-breaking Arctic oscillation and ozone loss. *Journal of Geophysical Research: Atmospheres*, *125*, e2020JD033271. <https://doi.org/10.1029/2020JD033271>
- Livesey, N. J., Read, W. G., Wagner, P. A., Froidevaux, L., Lambert, A., Manney, G. L., et al. (2020). *Earth Observing System (EOS) Aura Microwave Limb Sounder (MLS) version 4.2 × level 2 and 3 data quality and description document, JPL-D 33509 Rev. E*. Jet Propulsion Laboratory.
- Manney, G. L., Livesey, N. J., Santee, M. L., Froidevaux, L., Lambert, A., Lawrence, Z. D., et al. (2020). Record-low Arctic stratospheric ozone in 2020: MLS observations of chemical processes and comparisons with previous extreme winters. *Geophysical Research Letters*, *47*, e2020GL089063. <https://doi.org/10.1029/2020GL089063>
- Manney, G. L., Santee, M. L., Froidevaux, L., Hoppel, K., Livesey, N. J., & Waters, J. W. (2006). EOS MLS observations of ozone loss in the 2004–2005 Arctic winter. *Geophysical Research Letters*, *33*, L04802. <https://doi.org/10.1029/2005GL024494>
- Manney, G. L., Santee, M. L., Rex, M., Livesey, N. J., Pitts, M. C., Veefkind, P., et al. (2011). Unprecedented Arctic ozone loss in 2011. *Nature*, *478*, 469–475. <https://doi.org/10.1038/nature10556>
- Müller, R., Groöb, J.-U., Zafar, A. M., Robrecht, S., & Lehmann, R. (2018). The maintenance of elevated active chlorine levels in the Antarctic lower stratosphere through HCl null cycles. *Atmospheric Chemistry and Physics*, *18*, 2985–2997. <https://doi.org/10.5194/acp-18-2985-2018>
- Nakajima, H., Wohltmann, I., Wegner, T., Takeda, M., Pitts, M. C., Poole, L. R., et al. (2016). Polar stratospheric cloud evolution and chlorine activation measured by CALIPSO and MLS, and modeled by ATLAS. *Atmospheric Chemistry and Physics*, *16*, 3311–3325. <https://doi.org/10.5194/acp-16-3311-2016>
- Newman, P. A., Nash, E. R., & Rosenfield, J. E. (2001). What controls the temperature of the Arctic stratosphere during the spring? *Journal of Geophysical Research*, *106*(D17), 19999–20010. <https://doi.org/10.1029/2000JD000061>
- Oelhaf, H., Clarmann, T., Fischer, H., Friedl-Vallon, F., Fritzsche, C., Linden, A., et al. (1994). Stratospheric ClONO₂ and HNO₃ profiles inside the Arctic vortex from MIPAS-B limb emission spectra obtained during EASOE. *Geophysical Research Letters*, *21*, 1263–1266. <https://doi.org/10.1029/93GL01303>
- Pommereau, J.-P., Goutail, F., Pazmino, A., Lefèvre, F., Chipperfield, M. P., Feng, W., et al. (2018). Recent Arctic ozone depletion: Is there an impact of climate change? *Comptes Rendus Geoscience*, *350*(7), 347–353. <https://doi.org/10.1016/j.crte.2018.07.009>
- Portmann, R. W., Solomon, S., Garcia, R. R., Thomason, L. W., Poole, L. R., & McCormick, M. P. (1996). Role of aerosol variations in anthropogenic ozone depletion in the polar regions. *Journal of Geophysical Research*, *101*(D17), 22991–23006. <https://doi.org/10.1029/96JD02608>
- Prather, M. J. (1992). More rapid polar ozone depletion through the reaction of HOCl with HCl on polar stratospheric clouds. *Nature*, *355*(6360), 534–537. <https://doi.org/10.1038/355534a0>
- Randel, W. J., Wu, F., & Stolarski, R. (2002). Changes in column ozone correlated with the stratospheric EP flux. *Journal of the Meteorological Society of Japan*, *80*(4b), 849–862. <https://doi.org/10.2151/jmsj.80.849>
- Rex, M., Salawitch, R., von der Gathen, P., Harris, N. R. P., Chipperfield, M., & Naujokat, B. (2004). Arctic ozone loss and climate change. *Geophysical Research Letters*, *31*, L04116. <https://doi.org/10.1029/2003GL018844>
- Rex, M., Salawitch, R. J., Deckelmann, H., von der Gathen, P., Harris, N. R. P., Chipperfield, M. P., et al. (2006). Arctic winter 2005: Implications for stratospheric ozone loss and climate change. *Geophysical Research Letters*, *33*, L23808. <https://doi.org/10.1029/2006GL026731>
- Rex, M., von Der Gathen, P., Braathen, G., Harris, N., Reimer, E., Beck, A., et al. (1999). Chemical ozone loss in the Arctic winter 1994/95 as determined by the Match technique. *Journal of Atmospheric Chemistry*, *32*, 35–59. <https://doi.org/10.1023/A:1006093826861>
- Rieder, H. E., & Polvani, L. M. (2013). Are recent Arctic ozone losses caused by increasing greenhouse gases? *Geophysical Research Letters*, *40*, 4437–4441. <https://doi.org/10.1002/grl.50835>
- Schoeberl, M. R., Kawa, S. R., Douglass, A. R., McGee, T. J., Browell, E. V., Waters, J., et al. (2006). Chemical observations of a polar vortex intrusion. *Journal of Geophysical Research*, *111*, D20306. <https://doi.org/10.1029/2006JD007134>
- Sinnhuber, B.-M., Stiller, G., Ruhnke, R., von Clarmann, T., Kellmann, S., & Achmann, J. (2011). Arctic winter 2010/2011 at the brink of an ozone hole. *Geophysical Research Letters*, *38*, L24814. <https://doi.org/10.1029/2011GL049784>
- Smit, H. G. J., Straeter, W., Johnson, B. J., Oltmans, S. J., Davies, J., Tarasick, D. W., et al. (2007). Assessment of the performance of ECC-ozonesondes under quasi-flight conditions in the environmental simulation chamber: Insights from the Juelich Ozone Sonde Intercomparison Experiment (JOSIE). *Journal of Geophysical Research*, *112*, D19306. <https://doi.org/10.1029/2006JD007308>
- Solomon, S. (1999). Stratospheric ozone depletion: A review of concepts and history. *Reviews of Geophysics*, *37*(3), 275–316. <https://doi.org/10.1029/1999RG900008>
- Solomon, S., Haskins, J., Ivy, D. J., & Min, F. (2014). Fundamental differences between Arctic and Antarctic ozone depletion. *Proceedings of the National Academy of Sciences of the United States of America*, *111*(17), 6220–6225. <https://doi.org/10.1073/pnas.1319307111>
- Solomon, S., Kinnison, D., Bandoro, J., & Garcia, R. (2015). Simulation of polar ozone depletion: An update. *Journal of Geophysical Research: Atmospheres*, *120*, 7958–7974. <https://doi.org/10.1002/2015JD023365>
- Strahan, S. E., Douglass, A. R., & Newman, P. A. (2013). The contributions of chemistry and transport to low Arctic ozone in March 2011 derived from Aura MLS observations. *Journal of Geophysical Research: Atmospheres*, *118*, 1563–1576. <https://doi.org/10.1002/jgrd.50181>
- Tegtmeier, S., Rex, M., Wohltmann, I., & Krüger, K. (2008). Relative importance of dynamical and chemical contributions to Arctic winter-time ozone. *Geophysical Research Letters*, *35*, L17801. <https://doi.org/10.1029/2008GL034250>
- Tilmes, S., Müller, R., Engel, A., Rex, M., & Russell, J. M., III (2006). Chemical ozone loss in the Arctic and Antarctic stratosphere between 1992 and 2005. *Geophysical Research Letters*, *33*, L20812. <https://doi.org/10.1029/2006GL026925>
- von der Gathen, P., Kivi, R., Wohltmann, I., Salawitch, R. J., & Rex, M. (2021). Climate change favours large seasonal loss of Arctic ozone. *Nature Communications*, *12*, 3886. <https://doi.org/10.1038/s41467-021-24089-6>
- von der Gathen, P., & Maturilli, M. (2020). *Ozone sonde profiles during MOSAiC leg 1-2-3*. Alfred Wegener Institute—Research Unit Potsdam, PANGAEA. <https://doi.org/10.1594/PANGAEA.919538>
- WMO. (2018). *World Meteorological Organization (WMO)/United Nations Environment Programme (UNEP), Scientific assessment of ozone depletion: 2018* (Global Ozone Research and Monitoring Project—Report No. 58).

- Wohltmann, I., Lehmann, R., & Rex, M. (2010). The Lagrangian chemistry and transport model ATLAS: Simulation and validation of stratospheric chemistry and ozone loss in the winter 1999/2000. *Geoscientific Model Development*, 3, 585–601. <https://doi.org/10.5194/gmd-3-585-2010>
- Wohltmann, I., Lehmann, R., & Rex, M. (2017). A quantitative analysis of the reactions involved in stratospheric ozone depletion in the polar vortex core. *Atmospheric Chemistry and Physics*, 17, 10535–10563. <https://doi.org/10.5194/acp-17-10535-2017>
- Wohltmann, I., & Rex, M. (2009). The Lagrangian chemistry and transport model ATLAS: Validation of advective transport and mixing. *Geoscientific Model Development*, 2, 153–173. <https://doi.org/10.5194/gmd-2-153-2009>
- Wohltmann, I., von der Gathen, P., Lehmann, R., Maturilli, M., Deckelmann, H., Manney, G. L., et al. (2020). Near complete local reduction of arctic stratospheric ozone by severe chemical loss in spring 2020. *Geophysical Research Letters*, 47, e2020GL089547. <https://doi.org/10.1029/2020GL089547>